UICC
global cancer control

IJC
International Journal of Cancer

Synergistic antitumor activity of the SN-38-incorporating polymeric micelles NK012 with S-1 in a mouse model of non-small cell lung cancer

Tatsuya Nagano[1,2,3], Masahiro Yasunaga[1], Koichi Goto[2], Hirotsugu Kenmotsu[2], Yoshikatsu Koga[1], Jun-ichiro Kuroda[1], Yoshihiro Nishimura[3], Takashi Sugino[4], Yutaka Nishiwaki[2] and Yasuhiro Matsumura[1]

[1] Investigative Treatment Division, Research Center for Innovative Oncology, National Cancer Center Hospital East, 6-5-1 Kashiwanoha, Kashiwa, Chiba, Japan

[2] Thoracic Oncology Division, National Cancer Center Hospital East, 6-5-1 Kashiwanoha, Kashiwa, Chiba, Japan

[3] Division of Respiratory Medicine, Department of Internal Medicine, Kobe University Graduate School of Medicine, 7-5-1 Kusunokicho, Chuo-ku, Kobe, Hyogo, Japan

[4] Department of Pathology, Fukushima Medical University School of Medicine, 1 Hikariga-oka, Fukushima, Fukushima, Japan

The combination therapy of CPT-11, a prodrug of SN-38, with S-1, a dihydropyrimidine dehydrogenase inhibitory fluoropyrimidine, shows a high clinical response rate in non-small cell lung cancer (NSCLC). However, this combination causes severe toxicities such as diarrhea. Here, we investigated the advantages of treatment with the SN-38-incorporating polymeric micelles NK012 over CPT-11 in combination with S-1 in mice bearing a NSCLC xenograft in terms of antitumor activity and toxic effects, particularly intestinal toxicity. *In vitro* cytotoxic effects were examined in human NSCLC cell lines (A549, PC-9, PC-14, EBC-1 and H520). *In vivo* antitumor effects were evaluated in PC-14- and EBC-1-bearing mice after NK012 or CPT-11 administration on Days 0 and 7 and S-1 administration on Days 0–13. Pathological changes in the small intestine were also investigated. The *in vitro* growth inhibitory effects of NK012 were 56.8- to 622-fold more potent than those of CPT-11. NK012/S-1 treatment showed significantly higher antitumor activity both in PC-14-bearing ($p = 0.0007$) and EBC-1-bearing mice ($p < 0.0001$) than CPT-11/S-1 treatment. The deformity and decrease in the density of intestinal villi were more severe in CPT-11/S-1-treated mice than in NK012/S-1-treated mice. NK012/S-1 combination is a promising candidate regimen against NSCLC without inducing toxicities such as severe diarrhea and therefore warrants clinical evaluation.

Lung cancer is the leading cause of death from malignancies worldwide in both men and women,[1] and accounted for 31% (male) and 26% (female) of all cancer deaths in 2008.[2] It is histologically classified into small-cell lung cancer (SCLC) and non-small cell lung cancer (NSCLC). The standard first-line chemotherapy for NSCLC is platinum-based regimens.[3] However, as shown in a randomized phase III study, the response rate to these regimens is only 30–33% and the 1-year survival rate is 48–59%, with a median survival period of 11–14 months for advanced NSCLC patients with PS 0 or 1.[4] Therefore, the development of new chemotherapeutic agents and combination regimens against NSCLC is urgently desired.

Irinotecan hydrochloride (CPT-11), an anticancer drug, is converted to its biologically active metabolite 7-ethyl-10-hydroxy-camptothecin (SN-38) by carboxylesterases, and SN-38 has been shown to be efficacious against various human cancers such as colorectal, lung and ovarian cancer.[5–8] Although SN-38 has 1,000-fold more potent cytotoxic activity against various cancer cell lines *in vitro* than CPT-11,[9] its conversion rate from CPT-11 to SN-38 is <10% of the original CPT-11 dose in the body.[10,11]

On the other hand, the SN-38-incorporating polymeric micelles NK012 appear to have the advantage of passive targeting of the drug delivery system (DDS). In this passive DDS targeting, the drug accumulates in tumor tissue by utilizing the enhanced permeability and retention (EPR) effect.[12–15] This EPR effect is based on several pathological mechanisms that include hypervascularity, secretion of tumor vascular permeability factors stimulating extravasation of macromolecules including nanoparticles such as liposomes and micelles, and the absence of an effective lymphatic

Key words: NK012, S-1, diarrhea, drug delivery system, non-small cell lung cancer

Grant sponsor: Ministry of Education, Culture, Sports, Science and Technology (Scientific Research on Priority Areas); **Grant number:** 17016087; **Grant sponsors:** Third Term Comprehensive Control Research for Cancer, Japanese Foundation for Multidisciplinary Treatment of Cancer, Ministry of Health, Labor and Welfare; **Grant number:** H19-025

DOI: 10.1002/ijc.25282

History: Received 18 Dec 2009; Accepted 26 Jan 2010; Online 2 Mar 2010

Correspondence to: Yasuhiro Matsumura, Investigative Treatment Division, Research Center for Innovative Oncology, National Cancer Center Hospital East, 6-5-1 Kashiwanoha, Kashiwa, Chiba 277-8577, Japan, Tel.: +81-(0)-4-7133-1111(Ex: 5400), Fax: +81-(0)-4-7134-6866, E-mail: yhmatsum@east.ncc.go.jp

drainage of macromolecules accumulated in solid tumor tissue. In the previous study, we evaluated the antitumor effect by histopathologic evaluation and immunohistochemistry and demonstrated decreased cellularity, increased tumor stroma, and inflammatory cell infiltrations in the tumors treated with NK012. Tumors treated with CPT-11 showed no apparent morphologic differences from control tumors. Concordant with morphologic changes, the number of Ki-67 tumor cells tended to decrease in tumors treated with NK012 compared with CPT-11.[16] Recent studies demonstrated that NK012 is significantly more potent than CPT-11 against SCLC,[17] colorectal cancer,[18] renal cancer,[19] pancreatic cancer,[20] stomach cancer[21] and glioma.[22] Furthermore, in 2 independent phase I clinical trials in Japan[23] and the US,[24] nonhematological toxicities were minimal and grade 3/4 diarrhea, a major clinically important toxic effect or dose-limiting factor of CPT-11, was absent.

CPT-11 causes cell accumulation in the S phase, and 5-fluorouracil (5-FU) infusion induces DNA damage specifically in cells in the S phase.[25] Moreover, CPT-11 reduces thymidylate synthase (TS) and dihydropyrimidine dehydrogenase (DPD) mRNA expression,[26] and low gene expression level of TS and DPD had association with the response rate or chemosensitivity to 5-FU in metastatic colorectal cancer.[27,28] Recently, we demonstrated the higher synergistic antitumor activity of the NK012/5-FU combination against a colorectal tumor xenograft than the CPT-11/5-FU combination.[18] However, the use of an indwelling central venous catheter and a portable pump for 5-FU infusion may cause infection or thrombosis, and incur higher healthcare costs.[29]

S-1, on the other hand, is an oral anticancer agent composed of a 5-FU prodrug (tegafur), 5-chloro-2, 4-dihydroxypyrimidine (CDHP), and potassium oxonate (molar ratio = 1:0.4:1) and is categorized under DPD inhibitory fluoropyrimidines.[30] Tegafur generates 5-FU in the blood primarily *via* metabolism by liver enzyme cytochrome P450. CDHP enhances the serum 5-FU concentration by inhibiting the DPD activity competitively. Potassium oxonate is a reversible competitive inhibitor of orotate phosphoribosyl transferase, a phosphoenzyme for 5-FU and attributes to phosphorylation of 5-FU in the gastrointestinal tract and is expected to reduce the intestinal toxicity that is one of the clinical problems of 5-FU.[31]

In this context, we investigated the advantages of NK012/S-1 over CPT-11/S-1 in mice bearing a NSCLC xenograft in terms of antitumor activity and toxic effects, particularly intestinal toxicity.

Material and Methods

Drugs and cells

SN-38 and NK012 were prepared by Nippon Kayaku Co., (Tokyo, Japan). CPT-11 was purchased from Yakult Honsha Co., (Tokyo, Japan). S-1 was obtained from Taiho Pharmaceutical Co. (Tokyo, Japan). 5-FU was purchased from Kyowa Hakko (Tokyo, Japan).

The NSCLC cell lines A549, PC-9, PC-14, EBC-1 and H520 were purchased from the American Type Culture Collection (Rockville, MD). They were maintained in RPMI-1640 supplemented with 10% fetal bovine serum (Cell Culture Technologies, Gaggenau-Hoerden, Germany), penicillin, streptomycin and amphotericin B (100 units/mL, 100 μg/mL and 25 μg/mL, respectively; Sigma, St. Louis, MO) in a humidified atmosphere containing 5% CO_2 at 37°C.

In vitro growth inhibition assay

The growth inhibitory effects of NK012, CPT-11, SN-38 and 5-FU, instead of S-1 that is not suitable for use *in vitro*, because tegafur is a prodrug that is mainly activated in liver were examined by tetrazolum salt-based proliferation assay (WST-8 assay; Wako Chemicals, Osaka, Japan). A suspension (100 mL) of exponentially growing cells (1×10^5/mL) was placed into the wells of a 96-well plate and incubated for 24 hr at 37°C. Following medium removal, 100 μL of medium containing various concentrations of each drug was added to the wells and then incubated for 72 hr at 37°C. After medium removal, 10 μL of WST-8 solution and 90 μL of medium were added to the wells, followed by incubation for 1 hr at 37°C. The growth inhibitory effects of each drug were assessed spectrophotometrically (SpectraMax 190, Molecular Devices Corp., Sunnyvale, CA). IC_{50} was determined on the dose–response curves. The nature of interaction between NK012 and 5-FU against the NSCLC cell lines A549, PC-9, PC-14, EBC-1 and H520 was evaluated by median-effect plot analyses and the combination index method of Chou and Talalay.[32]

Reverse transcription and real-time PCR analysis

A suspension (2 mL) of exponentially growing cells (1×10^5/mL) was placed into the wells of a 6-well plate and incubated for 24 hr at 37°C. Following medium removal, 2 mL of medium and medium containing NK012 (1 μM) and CPT-11 (1 μM) were added to the wells and then incubated for 24 hr at 37°C ($n = 3$ for each arm), as reported.[33] Total RNA (1 μg) extracted from cells using an RNeasy Mini kit (Qiagen, Valencia, CA) was subjected to reverse transcription using the High Capacity cDNA Reverse Transcription kit (Applied Biosystems, Foster, CA). The resulting cDNA was then subjected to real-time PCR analysis using a Taqman PCR Reagent kit and an Applied Biosystems 7500 Fast Real-Time PCR System (Applied Biosystems). To quantify TS and DPD, we used TaqMan primers and a probe mixture (Applied Biosystems). Glyceraldehyde-3-phosphate dehydrogenase (GAPDH) mRNA was used as an internal control. Relative quantification of the total RNA in each sample was conducted using the comparative Ct (threshold cycle) method. The formulae for the relative quantification of each gene were as follows: (dCt of each gene) = (Ct of each gene) − (Ct of GAPDH), and (Relative quantification of each gene) = $2^{-(\text{dCt of each gene})}$.

Table 1. *In vitro* growth inhibitory activity of SN-38, NK012, CPT-11 and 5-FU in human non-small cell lung cancer cells

	IC50 (μmol/L)			
Cell line	SN-38	NK012	CPT-11	5-FU
A549	0.500 ± 0.092	0.888 ± 0.096	50.4 ± 2.3	419 ± 44
PC-9	0.0574 ± 0.0414	0.0732 ± 0.0020	8.86 ± 0.43	15.0 ± 4.2
PC-14	0.0488 ± 0.0011	0.0554 ± 0.0118	7.53 ± 4.97	2.99 ± 0.27
EBC-1	0.00374 ± 0.00449	0.00747 ± 0.00053	4.65 ± 0.17	45.8 ± 2.6
H520	0.0721 ± 0.0131	0.0773 ± 0.0071	9.10 ± 0.29	13.6 ± 7.1

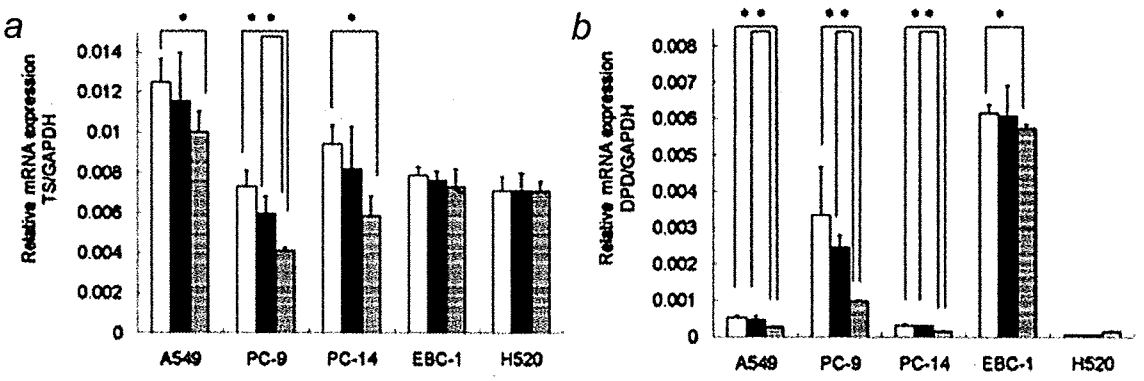

Figure 1. Effects of NK012 and CPT-11 on the expression of TS and DPD mRNA in non-small cell lung cancer (NSCLC) cell lines. (*a, b*) Downregulation of TS (*a*) and DPD (*b*) mRNA by NK012 and CPT-11 in NSCLC cell lines. A549, PC-9, PC-14, EBC-1 and H520 cells were incubated with medium containing 10% serum, medium containing NK012 (1 μmol/L) and 10% serum, and medium containing CPT-11 (1 μmol/L) and 10% serum for 24 hr. Then, total RNA was extracted from the cells and subjected to reverse transcription and real-time PCR analysis of TS and DPD mRNA. The amount of TS and DPD mRNA was normalized to that of glyceraldehyde-3-phosphate dehydrogenase mRNA. Bars, SD. *, $p < 0.05$. □, Medium; ■, CPT-11; ⊟, NK012.

Experimental mice model

Female BALB/c nude mice (6-weeks-old) were purchased from SLC Japan (Shizuoka, Japan). Mice were inoculated subcutaneously in the flank with 2.5×10^6 cells/50 μL cell suspension of PC-14 and 1.0×10^6 cells/50 μL cell suspension of EBC-1.

All animal procedures were performed in compliance with the guidelines for the care and use of experimental animals established by the Committee for Animal Experimentation of the National Cancer Center. These guidelines meet the ethical standards required by law and comply with the guidelines for the use of experimental animals in Japan.

In vivo growth inhibition assay

When the tumor volume (TV) reached 250 mm^3, mice were randomly divided into test groups consisting of 5 mice per group (Day 0). NK012, CPT-11, or NaCl solution (0.9%) was intravenously (i.v.) administered into the tail vein on Days 0 and 7. NK012 was administered at 5 mg/kg/d, which is 1/6 of the maximum tolerated dose (MTD). CPT-11 (reference drug) was administered at 10 mg/kg/d, which is also 1/6 of the MTD. S-1 was singularly or simultaneously administered by oral gavage once a day on Days 0–13 at 10 mg/kg/d, as reported.[34] NaCl solution (0.9%) was administered i.v. as normal control. The length (*a*) and width (*b*) of the tumor masses and body weight (BW) were measured twice a week, and TV was calculated using $TV = (a \times b^2)/2$. Relative tumor volume (RTV) on day n was calculated using $RTV = TV_n/TV_0$, where TV_n is the tumor volume on Day n and TV_0 is the tumor volume on Day 0. Relative body weight (RBW) was calculated using $RBW = BW_n/BW_0$. We evaluated the feces of mice on Days 4, 11 and 18 and considered soft, wet and canescent feces to indicate diarrhea, as reported.[35]

Experiment 1. Evaluation of the synergistic effects of NK012 with S-1. NK012, S-1, NK012/S-1, or NaCl solution (0.9%) was administered following the above dose schedules. We evaluated the effects of NK012/S-1 by comparing the data between NK012/S-1 and the additive effect (expected RTV). Expected RTV was calculated using (RTV of NK012) × (RTV of S-1) / (RTV of control), as reported.[36]

Experiment 2. Comparison of the antitumor effects of NK012/S-1 and CPT-11/S-1. NK012/S-1, CPT-11/S-1, or NaCl solution (0.9%) was administered following the above dose schedules. Two-way analysis of variance (ANOVA) was performed to compare the transitional RTV between NK012/S-1-treated mice and CPT-11/S-1-treated mice.

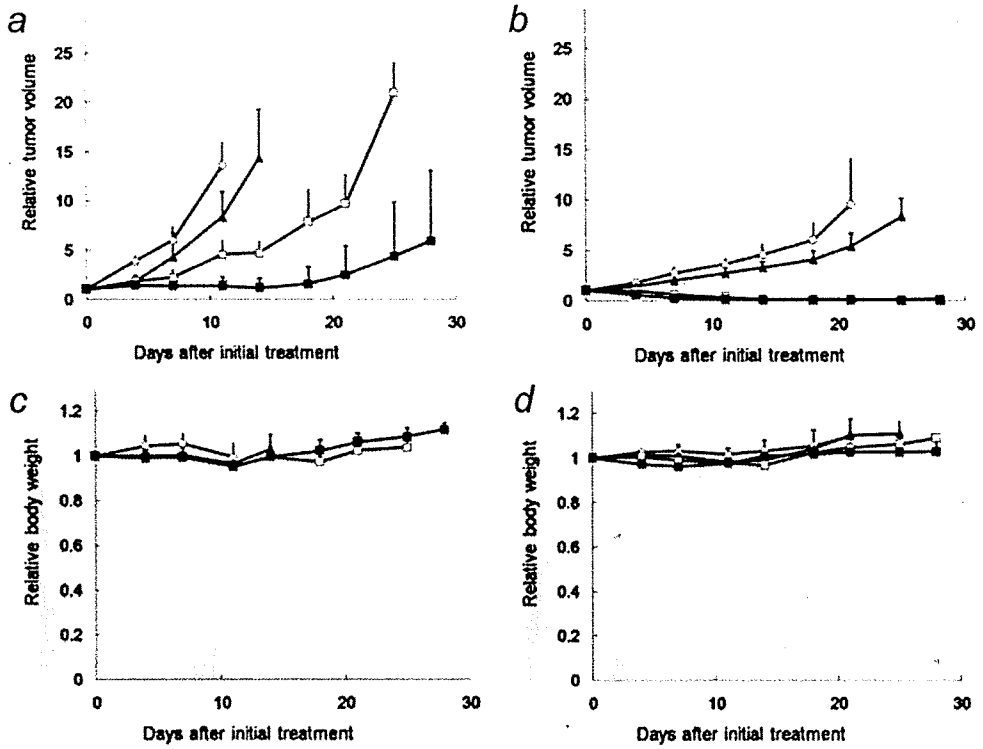

Figure 2. Growth inhibitory effects of NK012, S-1 and NK012/S-1 on PC-14 and EBC-1 tumor xenografts. (*a*, *b*) Relative tumor volume in mice treated with NK012, S-1 and NK012/S-1. PC-14 (*a*, *c*) and EBC-1 (*b*, *d*) cells were inoculated subcutaneously into the flank of mice, as described in Material and Methods. Drug administration was as follows: NK012 (5 mg/kg/d) on Days 0 and 7 (□), S-1 (10 mg/kg/d) on Days 0–13 (▲), NK012 (5 mg/kg/d) on Days 0 and 7 and combined with S-1 (10 mg/kg/d) on Days 0–13 (■), or NaCl solution (0.9%) on Days 0 and 7 as normal control (○). Points, mean; bars, SD. *, $p < 0.05$. (*c*, *d*) Treatment-related body weight loss occurred in mice treated with each drug. Points, mean; bars, SD.

Pathological studies of small intestinal mucosa

NaCl solution, CPT-11, NK012, S-1, CPT-11/S-1 and NK012/S-1 were administered to female BALB/c nude mice ($n = 3$) following the same dose schedules as those used in the treatment experiment. On Day 7 after the last dozing, mice were sacrificed and the small intestine was sampled at the middle portion. Samples were fixed in 10% formalin, paraffin-embedded, sectioned and stained with H&E. Villi density was defined as the number of villi per mm. We also evaluated the fecal condition mice on Days 4, 11 and 18. The extent of diarrhea as well as the appearance and number of villi was scored by independent, 2 blinded researchers.

Statistical analysis

Data were analyzed with Student's *t*-test when groups showed equal variances (*F* test) or Welch's test when they showed unequal variances (*F* test). ANOVA was performed to compare transitional RTV. Differences in the number of mice with diarrhea between NK012/S-1-treated mice and CPT-11/S-1-treated mice were tested for significance using the Pearson χ^2 test or Fisher exact test. All analyses were performed using StatView 5.0, and $p < 0.05$ was considered significant. All statistical tests were 2 sided, and data were expressed as mean ± SD.

Results

Sensitivity of NSCLC cells to NK012, CPT-11, SN-38 and S-1

The IC_{50} values of NK012 for the NSCLC cell lines ranged from 0.00747 μmol/L (EBC-1) to 0.888 μmol/L (A549) (Table 1). The cytotoxic effects of NK012 were 56.8- to 622-fold higher than those of CPT-11, whereas those of NK012 were 1.07- to 2.00-fold lower than those of SN-38. These features were comparable to those reported previously.[17,37] The molar ratios of NK012: 5-FU of 1:500 in A549, 1:200 in PC-9 and H520, 1:50 in PC-14, and 1:6,000 in EBC-1 were used for the drug combination studies based on the IC_{50} values of NK012 and 5-FU (Table 1). The synergic to additive effect between NK012 and 5-FU was observed in these NSCLC cell lines (data not shown).

Effects of NK012 and CPT-11 on the expression of TS and DPD mRNA in NSCLC cell lines

NK012 induced a significant decrease in TS mRNA expression in A549, PC-9 and PC-14 ($p = 0.0487$, $p = 0.0027$ and $p = 0.0095$, respectively) compared with the control, as well as in PC-9 ($p = 0.0225$) compared with CPT-11. NK012 also tended to decrease TS mRNA expression in EBC-1 and H520 compared with the control and CPT-11 (Fig. 1*a*). NK012

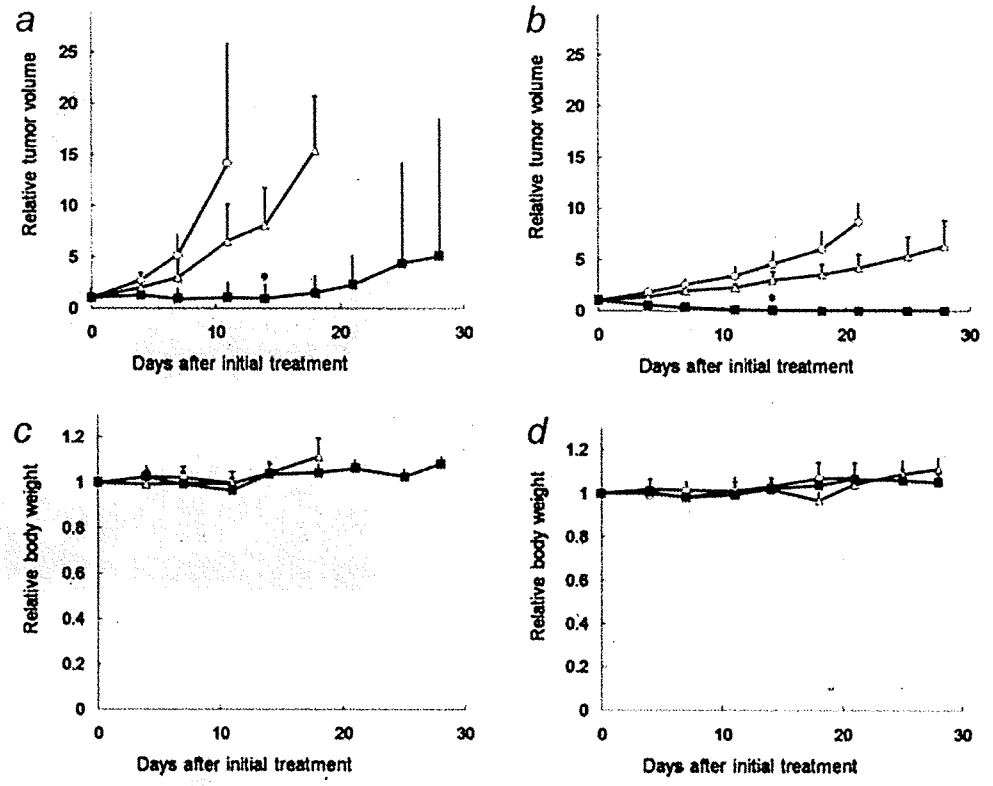

Figure 3. Antitumor effect of combined NK012/S-1 and CPT-11/S-1 treatment on PC-14 and EBC-1 tumor xenografts. (*a*, *b*) Relative tumor volume in mice treated with NK012/S-1 or CPT-11/S-1. PC-14 (*a*, *c*) and EBC-1 (*b*, *d*) cells were inoculated subcutaneously into the flank of mice, as described in Material and Methods. Drug administration was as follows: NK012 (5 mg/kg/d) on Days 0 and 7 and combined with S-1 (10 mg/kg/d) on Days 0–13 (■), CPT-11 (10 mg/kg/d) on Days 0 and 7 and combined with S-1 (10 mg/kg/d) on Days 0–13 (△), or NaCl solution (0.9%) on Days 0 and 7 as normal control (○). Points, mean; bars, SD. *, $p < 0.05$. (*c*, *d*) Treatment-related body weight loss occurred in each treated-mouse. Points, mean; bars, SD.

Table 2. Diarrhea after i.v. administrations of drugs

	Control	S-1	NK012	S-1 + NK012	CPT-11	S-1 + CPT-11
Day 4	0/24 (0)	1/13 (7.7)	0/10 (0)	1/24 (4.2)	0/4 (0)	3/14 (21.4)
Day 11	0/24 (0)	2/13 (15.4)	0/10 (0)	6/24 (25)	0/4 (0)	7/14 (50.0)
Day 18	0/24 (0)	0/13 (0)	0/10 (0)	2/24 (8.3)	0/4 (0)	3/14 (21.4)

Values in parentheses indicate percentage.

induced a significant decrease in DPD mRNA expression in A549, PC-9, PC-14 and EBC-1 ($p = 0.0019$, $p = 0.0358$, $p = 0.0020$ and $p = 0.0399$, respectively) compared with the control, as well as in A549, PC-9 and PC-14 ($p = 0.0373$, $p = 0.0013$ and $p = 0.0001$, respectively) compared with CPT-11. NK012 also tended to decrease DPD mRNA expression in EBC-1 compared with CPT-11, but not in H520 (Fig. 1*b*).

Antitumor activity of S-1, NK012, NK012/S-1, CPT-11 and CPT-11/S-1 against PC-14 and EBC-1 tumors

The therapeutic effect of NK012/S-1 was significantly superior to that of NK012 both in PC-14 ($p = 0.0013$) (Fig. 2*a*) and EBC-1 ($p = 0.0017$) (Fig. 2*b*), and this combination demonstrated a synergistic efficacy. The complete response rates achieved with NK012 and NK012/S-1 were 0 and 20% for PC-14 and 40 and 100% for EBC-1, respectively. Although treatment-related BW loss was observed in mice treated with each drug combination, BW recovered to the normal level in each group by Day 21 (Figs. 2*c* and 2*d*).

The therapeutic effect of NK012/S-1 was significantly superior to that of CPT-11/S-1 in PC-14-bearing ($p = 0.0007$) (Fig. 3*a*) and EBC-1-bearing mice ($p < 0.0001$) (Fig. 3*b*). The complete response rates achieved with NK012/S-1 were 40 and 100% for PC-14 and EBC-1, respectively. Although slight treatment-related BW loss was observed in mice treated with each drug combination, there was no significant difference between NK012/S-1 and CPT-11/S-1, and BW recovered to the normal level in each group by Day 21 (Figs. 3*c* and 3*d*).

Intestinal toxicity of CPT-11, NK012, S-1, CPT-11/S-1 and NK012/S-1

The mice treated with NaCl solution (0.9%), CPT-11, and NK012 had no diarrhea, whereas those treated with S-1, CPT-11/S-1 and NK012/S-1 had diarrhea (Table 2). The mice treated with CPT-11/S-1 tended to have higher incidence of diarrhea than those treated with S-1 ($p = 0.596$ Day 4, $p = 0.103$ Day 11, and $p = 0.222$ Day 18) or NK012/S-1 ($p = 0.132$ Day 4, $p = 0.163$ Day 11, and $p = 0.337$ Day 18).

The small intestinal mucosa of mice on Day 7 after the last treatment with NaCl solution (0.9%), CPT-11, and NK012 showed regular alignment of normal villi (Fig. 4). On the other hand, the small intestinal mucosa of mice treated with S-1, CPT-11/S-1 and NK012/S-1 showed deformation of villi, specifically a decrease in height and width. In particular, mice treated with CPT-11/S-1 showed more severe deformation and decrease in height and width of villi, as well as a more severe decrease in villi density than those treated with S-1 and NK012/S-1. Furthermore, CPT-11/S-1 treatment decreased villi density the most under the microscopic observation (Fig. 4*b*).

Discussion

The present study showed the synergistic effect between NK012 and S-1 and the significant antitumor activity of NK012/S-1 compared with CPT-11/S-1, the latter being one of the promising combinations against several cancers including NSCLC.[38] Indeed, CPT-11 combined with S-1 also exhibits potentially promising clinical activity with favorable toxic profile not only in NSCLC, but also advanced colorectal cancer,[29] and metastatic advanced gastric cancer.[39] Previously, we studied the differences in the effects between NK012 and CPT-11 on the cell cycle and demonstrated that NK012 induced a more prolonged accumulation of tumor cells in the S phase than CPT-11,[18] and this may explain the higher synergistic effect of NK012/5-FU than CPT-11/5-FU. Here, NK012 caused a larger decrease in TS and DPD mRNA expression than CPT-11. TS and DPD mRNA is thought to be associated with fluoropyrimidine sensitivity in lung cancer,[40] and a greater synergistic effect is expected between NK012 and fluoropyrimidines than between CPT-11 and fluoropyrimidines. In a phase II study of CPT-11/S-1 for advanced NSCLC, the grade 3/4 hematologic toxicities observed included neutropenia (25%), thrombocytopenia (3.6%) and anemia (3.6%), and the most common grade 3/4 nonhematologic toxicities were anorexia (14.3%), fatigue (8.9%) and diarrhea (8.9%).[38] Severe late-onset diarrhea is a major clinically important toxic effect or dose-limiting factor of CPT-11.[41–43] Diarrhea is also a clinical problem in S-1 treatment.[44] We previously demonstrated that a large amount of CPT-11 was excreted into the feces and high CPT-11 concentration was detected in the small intestinal epithelium. In contrast, a small amount of NK012 was found in the feces and NK012 was weakly and uniformly distributed in the mucosal interstitium. Furthermore, inflammatory changes in the small intestinal mucosa were rare in all NK012-treated mice, but were commonly observed in CPT-11-treated mice.[45] Here, in the present study, we used the same nude mice bearing human tumor xenografts in order to compare the present data with the previous data and demonstrated CPT-11/S-1 treatment induced more severe deformation of villi,

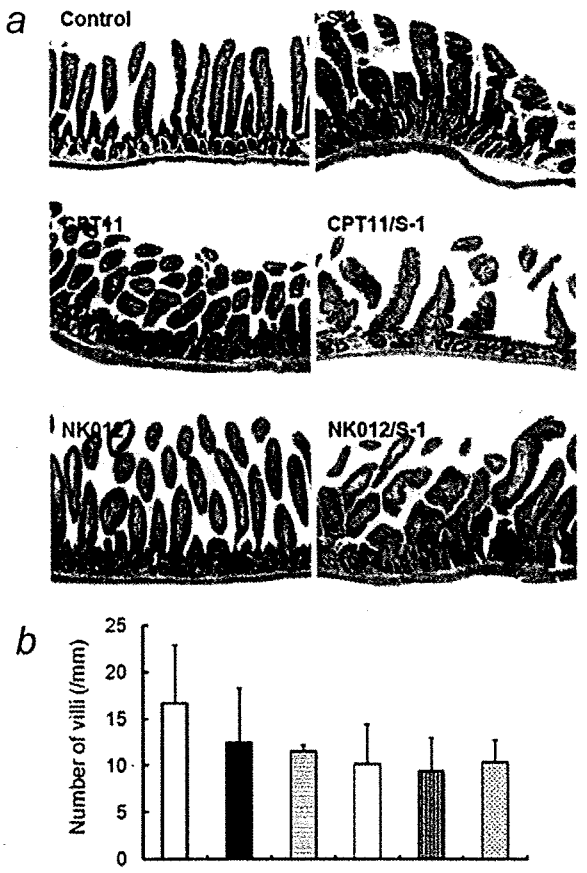

Figure 4. Pathological findings in intestinal mucosa. Mice were administered the following: NaCl solution (0.9%) on Days 0 and 7 as normal control, CPT-11 (10 mg/kg/d) on Days 0 and 7, NK012 (5 mg/kg/d) on Days 0 and 7, S-1 (10 mg/kg/d) on Days 0–13, CPT-11 (10 mg/kg/d) on Days 0 and 7 and combined with S-1 (10 mg/kg/d) on Days 0–13, or NK012 (5 mg/kg/d) on Days 0 and 7 and combined with S-1 (10 mg/kg/d) on Days 0–13. (*a*) Mice were sacrificed on Day 21 and the small intestine was sampled at the middle portion. Samples were fixed in 10% formalin, paraffin-embedded, sectioned and stained with H&E. In the NaCl-, CPT-11- and NK012-treated mice, the small intestinal mucosa showed regular alignment of normal villi. In the S-1- and NK012/S-1-treated mice, the small intestinal mucosa showed deformation of villi, specifically decreased height and width. This was also observed in CPT-11/S-1-treated mice with accompanying severe decrease in villi density. (*b*) Villi density indicates the number of villi per mm. Villi density was decreased the most with CPT-11/S-1 treatment. □, NaCl solution; ■, CPT-11; ⊟, NK012; ⊡, S-1; ◫, CPT-11/S-1; ▨, NK012 /S-1.

specifically decreased height and width, and severe decrease in villi density than NK012/S-1. Furthermore, villi density in CPT-11/S-1-treated mice was less than that in NK012/S-1-treated mice. The incidence of CPT-11/S-1-induced diarrhea was higher than that of NK012/S-1-induced diarrhea, although the difference was not significant ($p = 0.132$–0.337). There was no significant difference in other toxic effects including bone marrow and liver toxicities between NK012/S-1 and CPT-11/S-1 in the present treatment schedule (data not shown).

In conclusion, NK012/S-1 showed a significantly higher antitumor activity with less intestinal damage than CPT-11/S-1, one of the promising regimens against NSCLC, advanced colorectal cancer and metastatic advanced gastric cancer. Phase II clinical trials of NK012 monotherapy are now underway in patients with colorectal cancer in Japan and patients with triple negative breast cancer or SCLC in the USA. The present results suggest the clinical evaluation of NK012/S-1 in NSCLC patients.

Acknowledgements

This work was supported partly by a Grant-in-Aid from the Third Term Comprehensive Control Research for Cancer, the Ministry of Health, Labor and Welfare (Goto, Nishiwaki, and Matsumura), Scientific Research on Priority Areas from the Ministry of Education, Culture, Sports, Science and Technology (Matsumura), and the Japanese Foundation for Multidisciplinary Treatment of Cancer (Matsumura). The authors thank Ms. N. Mie and Ms. M. Ohtsu for technical assistance and Ms. K. Shiina and Ms. K. Abe for secretarial assistance.

References

1. Spiro SG, Porter JC. Lung cancer—where are we today? Current advances in staging and nonsurgical treatment. *Am J Respir Crit Care Med* 2002;166:1166–96.
2. Jemal A, Siegel R, Ward E, Hao Y, Xu J, Murray T, Thun MJ. Cancer statistics, 2008. *CA Cancer J Clin* 2008;58:71–96.
3. Schiller JH, Harrington D, Belani CP, Langer C, Sandler A, Krook J, Zhu J, Johnson DH. Comparison of four chemotherapy regimens for advanced non-small-cell lung cancer. *N Engl J Med* 2002;346:92–8.
4. Ohe Y, Ohashi Y, Kubota K, Tamura T, Nakagawa K, Negoro S, Nishiwaki Y, Saijo N, Ariyoshi Y, Fukuoka M. Randomized phase III study of cisplatin plus irinotecan versus carboplatin plus paclitaxel, cisplatin plus gemcitabine, and cisplatin plus vinorelbine for advanced non-small-cell lung cancer: Four-Arm Cooperative Study in Japan. *Ann Oncol* 2007;18:317–23.
5. Argiris A, Murren JR. Advances in chemotherapy for small cell lung cancer: single-agent activity of newer agents. *Cancer J* 2001;7:228–35.
6. Bodurka DC, Levenback C, Wolf JK, Gano J, Wharton JT, Kavanagh JJ, Gershenson DM. Phase II trial of irinotecan in patients with metastatic epithelial ovarian cancer or peritoneal cancer. *J Clin Oncol* 2003;21:291–7.
7. Cunningham D, Pyrhonen S, James RD, Punt CJ, Hickish TF, Heikkila R, Johannesen TB, Starkhammar H, Topham CA, Awad L, Jacques C, Herait P. Randomised trial of irinotecan plus supportive care versus supportive care alone after fluorouracil failure for patients with metastatic colorectal cancer. *Lancet* 1998;352:1413–18.
8. Negoro S, Masuda N, Takada Y, Sugiura T, Kudoh S, Katakami N, Ariyoshi Y, Ohashi Y, Niitani H, Fukuoka M. Randomised phase III trial of irinotecan combined with cisplatin for advanced non-small-cell lung cancer. *Br J Cancer* 2003;88:335–41.
9. Mathijssen RH, van Alphen RJ, Verweij J, Loos WJ, Nooter K, Stoter G, Sparreboom A. Clinical pharmacokinetics and metabolism of irinotecan (CPT-11). *Clin Cancer Res* 2001;7:2182–94.
10. Rothenberg ML, Kuhn JG, Burris HA, III, Nelson J, Eckardt JR, Tristan-Morales M, Hilsenbeck SG, Weiss GR, Smith LS, Rodriguez GI, Rock MK, Von Holf DD. Phase I and pharmacokinetic trial of weekly CPT-11. *J Clin Oncol* 1993;11:2194–204.
11. Slatter JG, Schaaf LJ, Sams JP, Feenstra KL, Johnson MG, Bombardt PA, Cathcart KS, Verburg MT, Pearson LK, Compton LD, Miller LL, Baker DS, et al. Pharmacokinetics, metabolism, and excretion of irinotecan (CPT-11) following I.V. infusion of [(14)C]CPT-11 in cancer patients. *Drug Metab Dispos* 2000;28:423–33.
12. Dvorak HF, Nagy JA, Dvorak JT, Dvorak AM. Identification and characterization of the blood vessels of solid tumors that are leaky to circulating macromolecules. *Am J Pathol* 1988;133:95–109.
13. Maeda H, Matsumura Y. Tumoritropic and lymphotropic principles of macromolecular drugs. *Crit Rev Ther Drug Carrier Syst* 1989;6:193–210.
14. Matsumura Y, Maeda H. A new concept for macromolecular therapeutics in cancer chemotherapy: mechanism of tumoritropic accumulation of proteins and the antitumor agent smancs. *Cancer Res* 1986;46:6387–92.
15. Matsumura Y, Maruo K, Kimura M, Yamamoto T, Konno T, Maeda H. Kinin-generating cascade in advanced cancer patients and in vitro study. *Jpn J Cancer Res* 1991;82:732–41.
16. Kuroda J, Kuratsu J, Yasunaga M, Koga Y, Kenmotsu H, Sugino T, Matsumura Y. Antitumor effect of NK012, a 7-ethyl-10-hydroxycamptothecin-incorporating polymeric micelle, on U87MG orthotopic glioblastoma in mice compared with irinotecan hydrochloride in combination with bevacizumab. *Clin Cancer Res* 2010;16:521–9.
17. Koizumi F, Kitagawa M, Negishi T, Onda T, Matsumoto S, Hamaguchi T, Matsumura Y. Novel SN-38-incorporating polymeric micelles, NK012, eradicate vascular endothelial growth factor-secreting bulky tumors. *Cancer Res* 2006;66:10048–56.
18. Nakajima TE, Yasunaga M, Kano Y, Koizumi F, Kato K, Hamaguchi T, Yamada Y, Shirao K, Shimada Y, Matsumura Y. Synergistic antitumor activity of the novel SN-38-incorporating polymeric micelles, NK012, combined with 5-fluorouracil in a mouse model of colorectal cancer, as compared with that of irinotecan plus 5-fluorouracil. *Int J Cancer* 2008;122:2148–53.
19. Sumitomo M, Koizumi F, Asano T, Horiguchi A, Ito K, Asano T, Kakizoe T, Hayakawa M, Matsumura Y. Novel SN-38-incorporated polymeric micelle, NK012, strongly suppresses renal cancer progression. *Cancer Res* 2008;68:1631–5.
20. Saito Y, Yasunaga M, Kuroda J, Koga Y, Matsumura Y. Enhanced distribution of NK012, a polymeric micelle-encapsulated SN-38, and sustained release of SN-38 within tumors can beat a hypovascular tumor. *Cancer Sci* 2008;99:1258–64.
21. Eguchi Nakajima T, Yanagihara K, Takigahira M, Yasunaga M, Kato K, Hamaguchi T, Yamada Y, Shimada Y, Mihara K, Ochiya T, Matsumura Y. Antitumor effect of SN-38-releasing polymeric micelles, NK012, on spontaneous peritoneal metastases from orthotopic gastric cancer in mice compared with irinotecan. *Cancer Res* 2008;68:9318–22.

22. Kuroda J, Kuratsu J, Yasunaga M, Koga Y, Saito Y, Matsumura Y. Potent antitumor effect of SN-38-incorporating polymeric micelle, NK012, against malignant glioma. *Int J Cancer* 2009;124:2505–11
23. Kato K, Hamaguchi T, Shirao K, Shimada Y, Doi T, Ohtsu A, Matsumura Y, Yamada Y. Interim analysis of phase I study of NK012, polymer micelle SN-38, in patients with advanced cancer. *Proc Am Soc Clin Oncol* 2008 (Abstract No. 485).
24. Burris HA, III, Infante JR, Spigel DR, Greco FA, Thompson DS, Matsumoto S, Kawamura S, Jones SF. A phase I dose-escalation study of NK012. *Proc Am Soc Clin Oncol* 2008 (Abstract No. 2538).
25. Azrak RG, Cao S, Slocum HK, Toth K, Durrani FA, Yin MB, Pendyala L, Zhang W, McLeod HL, Rustum YM. Therapeutic synergy between irinotecan and 5-fluorouracil against human tumor xenografts. *Clin Cancer Res* 2004;10: 1121–9.
26. Takiuchi H, Kawabe S-i, Gotoh M, Katsu K-i. Thymidylate synthase gene expression in primary tumors predicts activity of S-1-based chemotherapy for advanced gastric cancer. *Gastrointest Cancer Res* 2007;1: 171–6.
27. Salonga D, Danenberg KD, Johnson M, Metzger R, Groshen S, Tsao-Wei DD, Lenz HJ, Leichman CG, Leichman L, Diasio RB, Danenberg PV. Colorectal tumors responding to 5-fluorouracil have low gene expression levels of dihydropyrimidine dehydrogenase, thymidylate synthase, and thymidine phosphorylase. *Clin Cancer Res* 2000;6:1322–7.
28. Metzger R, Danenberg K, Leichman CG, Salonga D, Schwartz EL, Wadler S, Lenz HJ, Groshen S, Leichman L, Danenberg PV. High basal level gene expression of thymidine phosphorylase (platelet-derived endothelial cell growth factor) in colorectal tumors is associated with nonresponse to 5-fluorouracil. *Clin Cancer Res* 1998;4: 2371–6.
29. Goto A, Yamada Y, Yasui H, Kato K, Hamaguchi T, Muro K, Shimada Y, Shirao K. Phase II study of combination therapy with S-1 and irinotecan in patients with advanced colorectal cancer. *Ann Oncol* 2006;17:968–73.
30. Shirasaka T, Shimamoto Y, Fukushima M. Inhibition by oxonic acid of gastrointestinal toxicity of 5-fluorouracil without loss of its antitumor activity in rats. *Cancer Res* 1993;53:4004–9.
31. Muraoka A, Suehiro I, Fujii M, Nagata K, Kusunoki H, Kumon Y, Shirasaka D, Hosooka T, Murakami K. Acute gastric anisakiasis: 28 cases during the last 10 years. *Dig Dis Sci* 1996;41:2362–5.
32. Chou TC, Talalay P. Quantitative analysis of dose-effect relationships: the combined effects of multiple drugs or enzyme inhibitors. *Adv Enzyme Regul* 1984;22: 27–55.
33. Kamiyama H, Takano S, Tsuboi K, Matsumura A. Anti-angiogenic effects of SN38 (active metabolite of irinotecan): inhibition of hypoxia-inducible factor 1 α (HIF-1α)/vascular endothelial growth factor (VEGF) expression of glioma and growth of endothelial cells. *J Cancer Res Clin Oncol* 2005;131:205–13.
34. Okabe T, Okamoto I, Tsukioka S, Uchida J, Iwasa T, Yoshida T, Hatashita E, Yamada Y, Satoh T, Tamura K, Fukuoka M, Nakagawa K. Synergistic antitumor effect of S-1 and the epidermal growth factor receptor inhibitor gefitinib in non-small cell lung cancer cell lines: role of gefitinib-induced down-regulation of thymidylate synthase. *Mol Cancer Ther* 2008;7:599–606.
35. Brun Y, Wang XP, Willemot J, Sevenet T, Demenge P. Experimental study of antidiarrheal activity of Salicairine. *Fundam Clin Pharmacol* 1998;12:30–6.
36. Yokoyama Y, Dhanabal M, Griffioen AW, Sukhatme VP, Ramakrishnan S. Synergy between angiostatin and endostatin: inhibition of ovarian cancer growth. *Cancer Res* 2000;60:2190–6.
37. Uchino H, Matsumura Y, Negishi T, Koizumi F, Hayashi T, Honda T, Nishiyama N, Kataoka K, Naito S, Kakizoe T. Cisplatin-incorporating polymeric micelles (NC-6004) can reduce nephrotoxicity and neurotoxicity of cisplatin in rats. *Br J Cancer* 2005;93: 678–87.
38. Okamoto I, Nishimura T, Miyazaki M, Yoshioka H, Kubo A, Takeda K, Ebi N, Sugawara S, Katakami N, Fukuoka M, Nakagawa K. Phase II study of combination therapy with S-1 and irinotecan for advanced non-small cell lung cancer: west Japan thoracic oncology group 3505. *Clin Cancer Res* 2008;14: 5250–4.
39. Inokuchi M, Yamashita T, Yamada H, Kojima K, Ichikawa W, Nihei Z, Kawano T, Sugihara K. Phase I/II study of S-1 combined with irinotecan for metastatic advanced gastric cancer. *Br J Cancer* 2006; 94:1130–5.
40. Takechi T, Okabe H, Ikeda K, Fujioka A, Nakagawa F, Ohshimo H, Kitazato K, Fukushima M. Correlations between antitumor activities of fluoropyrimidines and DPD activity in lung tumor xenografts. *Oncol Rep* 2005;14:33–9.
41. Ohe Y, Sasaki Y, Shinkai T, Eguchi K, Tamura T, Kojima A, Kunikane H, Okamoto H, Karato A, Ohmatsu H, Kanzawa F, Saijo N. Phase I study and pharmacokinetics of CPT-11 with 5-day continuous infusion. *J Natl Cancer Inst* 1992;84:972–4.
42. Masuda N, Fukuoka M, Kusunoki Y, Matsui K, Takifuji N, Kudoh S, Negoro S, Nishioka M, Nakagawa K, Takada M. CPT-11: a new derivative of camptothecin for the treatment of refractory or relapsed small-cell lung cancer. *J Clin Oncol* 1992; 10:1225–9.
43. Ohno R, Okada K, Masaoka T, Kuramoto A, Arima T, Yoshida Y, Ariyoshi H, Ichimaru M, Sakai Y, Oguro M, Ito Y, Morishima Y, et al. An early phase II study of CPT-11: a new derivative of camptothecin, for the treatment of leukemia and lymphoma. *J Clin Oncol* 1990;8:1907–12.
44. Sakuramoto S, Sasako M, Yamaguchi T, Kinoshita T, Fujii M, Nashimoto A, Furukawa H, Nakajima T, Ohashi Y, Imamura H, Higashino M, Yamamura Y, et al. Adjuvant chemotherapy for gastric cancer with S-1, an oral fluoropyrimidine. *N Engl J Med* 2007;357:1810–20.
45. Nagano T, Yasunaga M, Goto K, Koga Y, Kuroda J-i, Nishimura Y, Sugino T, Nishiwaki Y, Matsumura Y. Antitumor activity of NK012 combined with cisplatin against small-cell lung cancer and intestinal mucosal changes in tumor-bearing mouse after treatment. *Clin Cancer Res* 2009;15: 4348–55.

Journal of Controlled Release 142 (2010) 245–250

Contents lists available at ScienceDirect

Journal of Controlled Release

journal homepage: www.elsevier.com/locate/jconrel

Cancer gene therapy by IL-12 gene delivery using liposomal bubbles and tumoral ultrasound exposure

Ryo Suzuki [a,1], Eisuke Namai [a,1], Yusuke Oda [a,1], Norihito Nishiie [a], Shota Otake [a], Risa Koshima [a], Keiichi Hirata [a], Yuichiro Taira [a], Naoki Utoguchi [a], Yoichi Negishi [b], Shinsaku Nakagawa [c], Kazuo Maruyama [a,*]

[a] Department of Biopharmaceutics, School of Pharmaceutical Sciences, Teikyo University, Sagamihara, Kanagawa, Japan
[b] Department of Drug and Gene Delivery System, School of Pharmacy, Tokyo University of Pharmacy and Life Science, Hachioji, Tokyo, Japan
[c] Department of Biotechnology and Therapeutics, Graduate School of Pharmaceutical Sciences, Osaka University, Suita, Osaka, Japan

ARTICLE INFO

Article history:
Received 24 August 2009
Accepted 26 October 2009
Available online 31 October 2009

Keywords:
Interleukin-12 (IL-12)
Ultrasound
Liposomes
Cancer gene therapy
Non-viral vector

ABSTRACT

Interleukin-12 (IL-12) gene therapy is expected to be effective against cancers because it primes the immune system for cancer cells. In this therapy, it is important to induce IL-12 gene expression in the tumor tissue. Sonoporation is an attractive technique for developing non-invasive and non-viral gene delivery systems, but simple sonoporation using only ultrasound is not an effective cancer gene therapy because of the low efficiency of gene delivery. We addressed this problem by combining ultrasound and novel ultrasound-sensitive liposomes (Bubble liposomes) which contain the ultrasound imaging gas perfluoropropane. Our previous work showed that this is an effective gene delivery system, and that Bubble liposome collapse (cavitation) is induced by ultrasound exposure. In this study, we assessed the utility of this system in cancer gene therapy using IL-12 corded plasmid DNA. The combination of Bubble liposomes and ultrasound dramatically suppressed tumor growth. This therapeutic effect was T-cell dependent, requiring mainly $CD8^+$ T lymphocytes in the effector phase, as confirmed by a mouse *in vivo* depletion assay. In addition, migration of $CD8^+$ T cells was observed in the mice, indicating that the combination of Bubble liposomes and ultrasound is a good non-viral vector system in IL-12 cancer gene therapy.

1. Introduction

Interleukin 12 (IL-12), a heterodimeric protein composed of p35 and p40 subunits [1,2], is produced by antigen-presenting cells such as dendritic cells and macrophages. IL-12 has a variety of immunomodulatory anti-tumor effects including induction of interferon-γ (IFN-γ secretion by stimulation of T cells and natural killer (NK) cells, and promotion of cytotoxic T lymphocyte (CTL) maturation [3,4]. In addition, IL-12 induces antiangiogenic effects mainly through IFN-γ-dependent production of the chemokine, interferon-inducible protein-10 (IP-10) [5], suggesting that IL-12 would be an effective anti-tumor agent. Although the systemic administration of IL-12 has been shown to suppress tumor growth, clinical trials were interrupted because of fatal adverse effects [6,7]. On the other hand, local administration of IL-12 into tumors is accepted as a more effective immunotherapeutic approach because of reduced systemic toxicity [8]. In particular, gene therapy by intratumoral injection of the IL-12 gene is expected to be an effective cancer therapy because it would lead to the locally sustained release of IL-12 in the tumor [9].

In cancer gene therapy, it is important to develop easy, safe, efficient and minimally-invasive techniques for transferring genes into tumor tissue. Non-viral gene therapy has many advantages over gene therapy, including ease of plasmid DNA production, lower toxicity and immunogenicity, and lower cost. Many researchers have attempted to develop non-viral gene delivery carriers such as lipids and polymers [10–13]. In addition, there is wide interest in the potential of therapeutic ultrasound for enhancing the efficiency of gene delivery [14,15]. In particular, a physical method using ultrasound combined with nano/microbubbles has many of the desired characteristics for an ideal gene therapy, including low toxicity, the potential for repeated applications, organ specificity, and broad applicability to acoustically accessible organs [16,17]. Ultrasound can create transient nonlethal perforations in cell membranes [18], allowing extracellular plasmid DNA to be directly delivered into the cytosol. The main mechanism of gene delivery is thought to be acoustic cavitation using nano/microbubbles as cavitation nuclei. Based on liposome technology, we previously developed novel liposomal bubbles (Bubble liposomes) containing lipid micelles of the ultrasound imaging gas, perfluoropropane [19–23]. When coupled with ultrasound exposure, Bubble liposomes could

* Corresponding author. 1091-1 Suwarashi, Sagamiko, Sagamihara, Kanagawa 229-0195, Japan. Tel.: +81 42 685 3724; fax: +81 42 685 3432.
E-mail address: maruyama@pharm.teikyo-u.ac.jp (K. Maruyama).
[1] The first three authors contributed equally to this work.

0168-3659/$ – see front matter © 2009 Elsevier B.V. All rights reserved.
doi:10.1016/j.jconrel.2009.10.027

be used as novel gene delivery agents *in vitro* and *in vivo* [19,20,24]. In addition, we found that gene delivery into femoral artery with this method was much more efficient than the conventional lipofection method using Lipofectamine 2000 [19]. And there is little report about cancer gene therapy using nano/microbubbles and ultrasound. Therefore, it is expected that gene delivery using Bubble liposomes and ultrasound will be an effective non-viral vector system for cancer gene therapy. In this study, we assessed this gene delivery system in cancer gene therapy using IL-12 gene.

2. Materials and methods

2.1. Cells and animals

Murine ovarian carcinoma OV-HM cells were kindly provided by Dr. Hiromi Fujiwara. An ovarian tumor OV2944, was induced in a female (C57BL/6 X C3H/He) F_1 mice by giving a single whole-body neutron irradiation, and a cloned line with highly metastatic property (designated OV-HM) was isolated from the parental line [25]. OV-HM cells were grown in RPMI-1640 (Sigma Chemical Co., St. Louis, MO) containing 100 U/ml penicillin (Wako Pure Chemical Industries, Osaka, Japan) and 100 μg/ml streptomycin (Wako Pure Chemical Industries) supplemented with 10% heat-inactivated fetal bovine serum (FBS, GIBCO, Invitrogen Co., Carlsbad, CA). B6C3F1 female mice were obtained from Sankyo Labo Service Corporation, Inc. (Tokyo, Japan) and used at 6 weeks of age. All of the experimental procedures were performed in accordance with the Teikyo University guidelines for the welfare of animals in studies of experimental neoplasia.

2.2. Preparation of Bubble liposomes

Liposomes composed of 1,2-distearoyl-sn-glycero-phosphatidylcholine (DSPC) (NOF Corp., Tokyo, Japan) and 1,2-distearoyl-sn-glycero-3-phosphatidyl-ethanolamine s-methoxypolyethyleneglycol (DSPE-PEG(2 k)-OMe, (PEG, Mw = ca. 2000); NOF) (94:6 (m/m)) were prepared by reverse phase evaporation. Briefly, all reagents (total lipid: 100 μmol) were dissolved in 8 ml of 1:1 (v/v) chloroform/diisopropyl ether, and then 4 ml of phosphate buffered saline (PBS) was added. The mixture was sonicated and evaporated at 65 °C. The organic solvent was completely removed, and the size of the liposomes was adjusted to less than 200 nm using an extruding apparatus (Northern Lipids Inc., Vancouver, Canada) and sizing filters (pore sizes: 100 and 200 nm; Nuclepore Track-Etch Membrane, Whatman plc, UK). After sizing, the liposomes were sterilized by passing them through a 0.45-μm pore size filter (Millex HV filter unit, Durapore PVDF membrane, Millipore Corp., MA). The size of the liposomes was measured by dynamic light scattering (ELS-800, Otsuka Electronics Co., Ltd., Osaka, Japan). The average diameter of these liposomes was between 150 and 200 nm. Lipid concentration was measured using the Phospholipid C test (Wako Pure Chemical Industries). Bubble liposomes were prepared from the liposomes and perfluoropropane gas (Takachiho Chemical Industrial Co., Ltd., Tokyo, Japan). Briefly, 5-ml sterilized vials containing 2 ml of the liposome suspension (lipid concentration: 2 mg/ml) were filled with perfluoropropane, capped, and then supercharged with 7.5 ml of perfluoropropane. The vial was placed in a bath-type sonicator (42 kHz, 100 W; Bransonic 2510 J-DTH, Branson Ultrasonics Co., Danbury, CT) for 5 min to form the Bubble liposomes. In this method, the liposomes were reconstituted by sonication and supercharged with perfluoropropane in the 5-mL vial container. Perfluoropropane was entrapped within the lipid micelles, comprising DSPC and DSPE-PEG (2 k)-OMe, to form nanobubbles. The lipid nanobubbles were encapsulated within the reconstituted liposomes, which now ranged in size from around 500 nm–1 μm, compared to 150–200 nm before supercharging with perfluoproropane.

2.3. Plasmid DNA vector construction

The plasmid pCMV-Luc contained the firefly luciferase gene of pGL3-control (Promega) at the *Hin*dIII/*Xba*I site of the pcDNA3 vector (Invitrogen). This plasmid was an expression vector encoding the firefly luciferase gene under the control of a cytomegalovirus promoter. The plasmid pCMV-IL12 contained murine IL-12, derived from mIL-12 BIA/pBluescript II KS(−) (kindly provided by Dr. Yamamoto, Department of Immunology, Graduate School of Pharmaceutical Sciences, Osaka University, Japan) in the *Xho*I/*Not*I site of the pHMCMV5 vector. This expression vector encoded the murine IL-12 gene under the control of a cytomegalovirus promoter [26].

2.4. Intratumoral administration of plasmid DNA

B6C3F1 mice were intradermally inoculated with OV-HM cells (1×10^6 cells/mouse) in the flank. After 7 days, a suspension (25 μL/mouse) of Bubble liposomes (2.5 μg) and pCMV-Luc or pCMV-IL12 (10 μg) was injected into the tumor, and ultrasound (1 MHz, 0.7 W/cm^2, 60 s) was transdermally applied to the tumor tissue. A conventional lipofection method was also investigated. A suspension (25 μL/mouse) of Lipofectamine 2000 (20 μg) and pCMV-Luc or pCMV-IL12 (10 μg) were incubated together for 20 min to allow them to complex. Then the complex was injected into the tumor. All treatment groups consisted of five mice.

2.5. Luciferase assay

Each day after the pCMV-Luc injection, mice were sacrificed and the tumor tissue was recovered. The tumor tissue was homogenized in lysis buffer (0.1% Triton X-100, 0.1 M Tris–HCl pH 7.8, 2 mM EDTA) and frozen (−80 °C) and thawed at room temperature twice. The homogenized tumor tissue was centrifuged (12,000 rpm, 4 °C, 10 min) and the supernatant was recovered for the luciferase assay. Luciferase activity was measured using a luciferase assay system (Promega) and luminometer (TD-20/20, Turner Designs, Sunnyvale, CA). The activity was measured as relative light units (RLU) per milligram protein.

2.6. Reverse transcription-polymerase chain reaction (RT-PCR) analysis for IL-12 expression in tumor tissues

OV-HM tumors were collected 1 or 2 days after intratumoral injection of pCMV-IL12 and Bubble liposomes, and total RNA was isolated using ISOGEN according to the manufacturer's instructions and dissolved with 20 μL TE buffer. RT proceeded for 60 min at 42 °C in 20 μl reaction mixture containing 1 μg total RNA treated with DNase I, 5 mM $MgCl_2$, RNA PCR buffer (Takara Bio, Kyoto, Japan), 1 mM dNTP mix, 0.125 μM Oligo dT-Adaptor primer (Takara Bio), 0.5 U/μL RNase inhibitor and 0.25 U/μL AMV reverse transcriptase XL (Takara Bio). PCR amplification of IL-12 and β-actin transcripts was performed in 20 μL reaction mixture containing 2 μL RT-material, PCR buffer, 0.5 U Takara Ex Taq HS, 0.2 mM dNTP, 2.5 mM $MgCl_2$, and 0.4 mM primers. The sequences of the specific primers were as follows: murine IL-12: forward, 5′-ctc acc tgt gac acg cct ga-3′; reverse, 5′-cag gac act gaa tac ttc tc-3′; and murine β-actin: forward, 5′-tgt gat ggt ggg aat ggg tca g-3′; reverse, 5′-ttt gat gtc acg cac gat ttc c-3′. After denaturation for 5 min at 95 °C, three sequential steps, denaturation for 45 s at 95 °C, annealing for 60 s at 48 °C, and extension for 2 min at 72 °C, were repeated for 40 cycles, with a final extension step for 4 min at 72 °C.

EZ Load (Bio-Rad Laboratories, Inc., Tokyo, Japan) was used as a 100-bp molecular ladder. The PCR products were electrophoresed through a 2% agarose gel, stained with ethidium bromide, and visualized under ultraviolet radiation. The expected PCR product sizes were 430 bp (IL-12) and 514 bp (β-actin).

2.7. Anti-tumor effect of intratumoral administration on IL-12 gene expression in mice

B6C3F1 mice were intradermally inoculated with OV-HM cells (1×10^6 cells/mouse) into the flank. For single therapy, established tumors with diameters of 8–10 mm were injected with a suspension (25 μL/mouse) of Bubble liposomes (2.5 μg) and pCMV-IL12 (10 μg), and ultrasound (1 MHz, 0.7 W/cm^2, 60 s) was transdermally applied to the tumor tissue. We also examined the intratumoral injection of a complex (25 μL/mouse) of Lipofectamine 2000 (20 μg) and pCMV-IL12 (10 μg) as a conventional lipofection method for comparison. For repetitive therapy, the mice were treated as above on days 0, 2, 5, 7, 9 and 12 after first treatment. The anti-tumor effects were evaluated by measuring tumor volume. Tumor volume was calculated using the formula: (major axis × minor axis^2) × 0.5. All data are expressed as relative tumor volume to that before the first treatment. All treated groups contained five mice.

2.8. In vivo depletion analysis

GK1.5 hybridoma (rat anti-mouse CD4 mAb) and 53-6.72 hybridoma (rat anti-mouse CD8 mAb) were purchased from American Type Culture Collection (ATCC) (Manassas, VA). Ascites from BALB/c nude mice intraperitoneally injected with each hybridoma were collected, and antibodies were purified using a protein A column (GE Healthcare, Pollards Wood, UK). Mice bearing OV-HM were intratumorally injected with pCMV-IL12 and Bubble liposomes on days 0, 2, 5, 7, 9 and 12 after the first treatment. Additionally, the mice were intraperitoneally injected four times on days −3, 4, 11 and 18 after the first treatment with 100 μg/mouse of anti-mouse CD8 mAb for CD8$^+$ cells or anti-mouse CD4 antibody for CD4$^+$ cells, or on days −3, −2, −1, 0, 5, 10, 15 and 20 after the first treatment with 200 μg/mouse of anti asialoGM1 mAb (Wako Pure Chemical Industries) for NK cells. The depletion of T-cell subsets and NK cells was confirmed by flow cytometric analysis of peripheral blood. Tumor growth was monitored as described above.

2.9. Immunohistochemical analysis

B6C3F1 mice were intradermally inoculated with OV-HM cells (1×10^6 cells/mouse) into the flank. After 7, 9 or12 days, a suspension (25 μL/mouse) of Bubble liposomes (2.5 μg) and pCMV-IL12 (10 μg) was injected into the tumor, and ultrasound (1 MHz, 0.7 W/cm^2, 60 s) was transdermally applied to the tumor tissue. After 13 days of tumor inoculation, the mice were sacrificed, and the tumor tissue was dissected and then embedded in the OCT compound. Frozen sections (10 μm thick) were fixed with 4% paraformaldehyde at 4 °C for 10 min, and treated with 0.3% H_2O_2 in methanol:PBS (1:1) for 15 min and 1.5% normal cow serum in PBS for 10 min at room temperature. The sections were treated with rat anti-mouse CD8 mAbs (1:100) or rat anti-mouse perforin mAbs (1:100) (Kamiya Biomedical Co., Seattle, WA) in PBS containing 0.1% BSA at 4 °C overnight. The section was washed and treated with horse radish peroxidase-conjugated goat anti-rat IgG Abs (1:500) in PBS containing 0.1% BSA at room temperature for 2 h. The diaminobenzidine-reaction system (Vector Laboratories, Burlingame, CA) was used to stain the sections. We also stained the sections with hematoxylin solution for counterstaining. The samples were observed with a microscope (IX-71, Olympus, Tokyo, Japan).

2.10. Statistical analysis

Differences between experimental groups were compared with non-repeated measures ANOVA and Dunnett's test.

3. Results

3.1. Bubble liposomes and ultrasound-mediated gene delivery into solid tumors

To evaluate the effectiveness of gene delivery with Bubble liposomes and ultrasound into OV-HM solid tumors, we utilized the luciferase reporter gene expression assay (Fig. 1a). The effectiveness of gene delivery with conventional lipofection using Lipofectamine 2000 was also examined. Luciferase expression with ultrasound or Bubble liposomes was low, and even lower with Lipofectamine 2000. On the other hand, luciferase expression with the combination of Bubble liposomes and ultrasound exposure was higher than in the other groups. Therefore, the profile of luciferase expression was measured in mice treated with Bubble liposomes and ultrasound. Luciferase expression gradually decreased after transfection (Fig. 1b), with the elimination rate constant (Ke) and half period ($T_{1/2}$) of gene expression being 1.26 days^{-1} and 0.54 days, respectively.

3.2. IL-12 gene expression in solid tumors transfected with IL-12 corded plasmid DNA using Bubble liposomes and ultrasound

To assess IL-12 expression in solid tumors transfected with IL-12 corded plasmid DNA (pCMV-IL12), the expression of IL-12p40 mRNA was examined with RT-PCR (Fig. 2). No expression of IL-12p40 mRNA in solid tumors transfected with pCMV-IL12 was observed. A small amount of IL-12p40 mRNA was expressed in solid tumors transfected with pCMV-IL12 using Lipofectamine 2000 on 1 day after gene transfection. On the other hand, the expression of IL-12p40 mRNA was observed in solid tumors transfected with pCMV-IL12 using Bubble liposomes and ultrasound for at least 2 days after gene transfection. This result indicates that IL-12 is expressed more effectively in solid tumors transfected using Bubble liposomes and ultrasound than using Lipofectamine 2000.

3.3. Anti-tumor effect of IL-12 gene delivery with Bubble liposomes and ultrasound

First, we examined the effect of a single delivery of IL-12 gene (Fig. 3a). Gene delivery using Bubble liposomes, ultrasound or

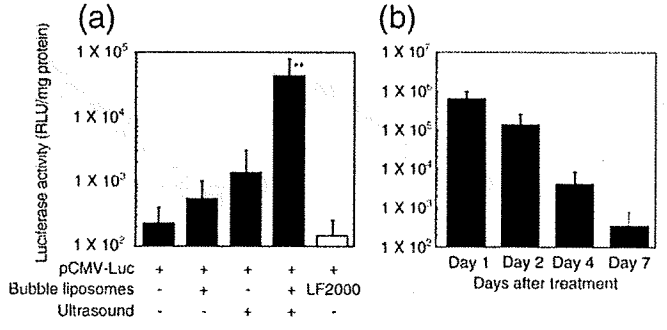

Fig. 1. Gene expression profiles in solid tumors following gene delivery with Bubble liposomes and ultrasound. Comparison of gene expression efficiency by gene delivery with each gene delivery method. B6C3F1 mice were intradermally inoculated with 1×10^6 OV-HM cells into the flank. Seven days after inoculation, the tumors were injected with pCMV-Luc (10 μg) using Bubble liposomes (2.5 μg) and/or ultrasound (1 MHz, 0.7 W/cm^2, 1 min), or Lipofectamine 2000 as a conventional lipofection method. (a) Two days after gene delivery, the mice were sacrificed and luciferase expression was measured in the solid tumor tissue. The data represent means ± SD ($n=3$). (b) Time course of luciferase expression after gene delivery with Bubble liposomes and ultrasound. Luciferase expression was measured at each time point after pCMV-Luc delivery into the solid tumor with Bubble liposomes and ultrasound exposure. $^{**}P<0.01$ compared to the group treated with plasmid DNA, Bubble liposomes, ultrasound or LF2000. LF2000: Lipofectamine 2000.

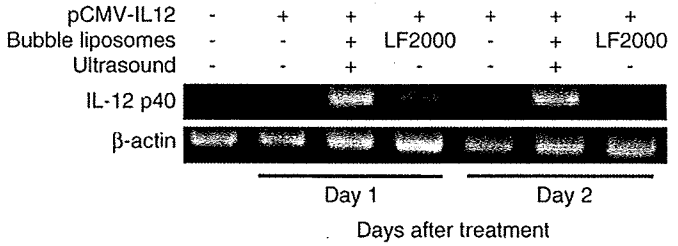

Fig. 2. RT-PCR analysis of IL-12 expression in solid tumors after pCMV-IL12 gene delivery. B6C3F1 mice were intradermally inoculated with 1×10^6 OV-HM cells into the flank. Seven days after inoculation, the tumors were injected with pCMV-IL12 (10 μg) using Bubble liposomes (2.5 μg) and/or ultrasound (1 MHz, 0.7 W/cm^2, 1 min), or Lipofectamine 2000 as a conventional lipofection method. One or 2 days after gene delivery, the mice were sacrificed, total RNA was prepared from the tumors, then RT-PCR was performed using a specific IL-12 primer as described in Materials and Methods. The PCR products were electrophoresed though a 3% agarose gel and stained with EtBr. To ensure the quality of the procedure, RT-PCR was performed on the same sample using a specific β-actin primer. LF2000: Lipofectamine 2000.

Lipofectamine 2000 showed no apparent anti-tumor effect, as was found for pCMV-Luc intratumoral delivery using Bubble liposomes and ultrasound. In contrast, the growth of OV-HM tumors was dramatically suppressed in mice treated by pCMV-IL12 intratumoral delivery using Bubble liposomes and ultrasound; however, complete regression was not observed. Thus, we examined the effect of repetitive IL-12 gene therapy to obtain more effective therapeutic effects (Fig. 3b). Gene delivery using Bubble liposomes, ultrasound or Lipofectamine 2000 showed no apparent anti-tumor effect, even in repetitive therapy. In contrast, IL-12 gene delivery using the combination of Bubble liposomes and ultrasound effectively suppressed tumors, and complete regression occurred in 80% of the tumor-bearing mice. There was no decrease in body weight of these mice as a side effect of IL-12 cancer therapy (data not shown). In addition, this group of mice demonstrated prolonged survival, indicating that OV-HM cells were effectively killed by IL-12 gene therapy with Bubble liposomes and ultrasound.

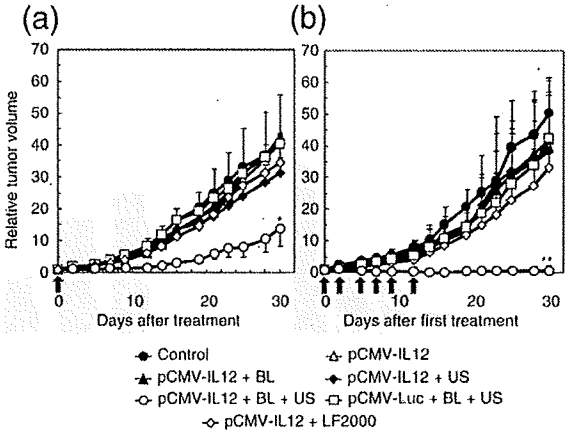

Fig. 3. Anti-tumor effect of IL-12 gene delivery. B6C3F1 mice were intradermally inoculated with 1×10^6 OV-HM cells into the flank. (a) Single gene therapy. (b) Repetitive gene therapy. Each day (arrows) after first treatment, the tumors were injected with pCMV-IL12 (10 μg) using Bubble liposomes (2.5 μg) and/or ultrasound (1 MHz, 0.7 W/cm^2, 1 min), or Lipofectamine 2000 as a conventional lipofection method. The volume of the growing tumors was calculated by: (tumor volume; mm^3) = (major axis; mm) × (minor axis; mm)^2 × 0.5). The data are represented as tumor volume relative to the tumor volume on the first day of treatment (day 7 after tumor inoculation). Arrow shows days of treatment. Each point represents the mean ± SD ($n = 5$). *$P < 0.05$ or **$P < 0.01$ compared to the group treated with pCMV-IL12, pCMV-IL12 + BL, US or LF2000 or pCMV-Luc + BL + US. BL: Bubble liposomes, US: Ultrasound, LF2000: Lipofectamine 2000.

3.4. Determination of immune subsets responsible for tumor regression induced by IL-12 gene delivery using Bubble liposomes and ultrasound

To investigate the anti-tumor mechanism of intratumoral pCMV-IL12 delivery using Bubble liposomes and ultrasound, we examined the individual contribution of CD4$^+$ and CD8$^+$ T cells and NK cells (Fig. 4). The anti-tumor effects of pCMV-IL12 delivery using Bubble liposomes and ultrasound were attenuated by the depletion of CD8$^+$ T cells and CD4$^+$ T cells. The depletion of CD8$^+$ T cells effectively blocked the anti-tumor effect. Also, the anti-tumor effect was blocked in mice that were depleted of both CD4$^+$ and CD8$^+$ T cells. On the other hand, the tumor growth suppressing effects were not affected by NK cell depletion. Therefore, we concluded that CD8$^+$ CTLs, activated by the helper function of CD4$^+$ T cells, were the predominant effector cells in this therapeutic system. CD4$^+$ cells alone also partly contributed to the enhanced anti-tumor effect.

To investigate the infiltration of CD8$^+$ T cells into tumor tissues containing the IL-12 gene delivered using Bubble liposomes and ultrasound, tumor tissues were subjected to immunohistochemical staining for CD8 (Fig. 5a–c). Tumor tissue from untreated mice, or mice treated with the IL-12 gene delivered using Bubble liposomes and ultrasound, showed increased accumulation of CD8$^+$ T cells compared to control mice treated with the luciferase gene, delivered using Bubble liposomes and ultrasound. In addition, we examined the activation states of tumor-infiltrating T cells by immunohistochemical analysis for perforin, the major cytotoxic molecule in activated CTLs (Fig. 5d–f). Tumor tissue to which the IL-12 gene had been delivered using Bubble liposomes and ultrasound exhibited significantly higher numbers of perforin-positive cells than non-treated tumor tissue, or tissue treated with luciferase gene.

4. Discussion

There are two main therapeutic strategies in cancer gene therapy. One approach is to cause a direct effect on cancer cells by delivering suicide genes such as herpes simplex virus thymidine kinase, [27] siRNA for oncogenes, [28] and proteins associated with the cell cycle [29] and apoptosis [30,31]. In this approach, it is necessary to deliver the therapeutic gene into most of the cancer cells to induce cytotoxicity. The second approach is indirect and activates anti-tumor immunity mediated by the delivery of a cytokine gene such as IL-12. In such cytokine gene therapy, the therapeutic gene does not have to be delivered into all the cancer cells since the cytokine is secreted from the cells. Therefore, a local supply of IL-12 in tumors is

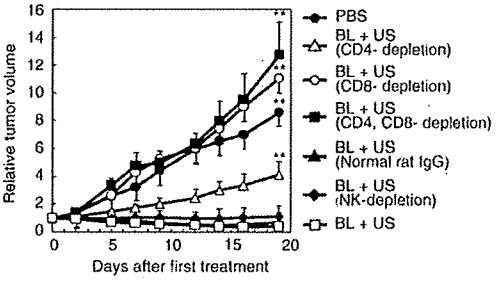

Fig. 4. Determination of immune subsets responsible for the anti-tumor effect induced by IL-12 gene delivery with Bubble liposomes and ultrasound. B6C3F1 mice were intradermally inoculated with 1×10^6 OV-HM cells into the flank. For depletion of CD4$^+$ T cells, CD8$^+$ T cells or NK cells in the mice, GK1.5 ascites (anti-CD4), 53-6.72 ascites (anti-CD8) or anti-asialoGM1 antisera was intraperitoneally injected as described in Materials and methods. On 0, 2, 5, 7, 9 or 12 days after first treatment, IL-12 gene therapy was performed with Bubble liposomes and ultrasound. The data represent the tumor volume relative to the tumor volume on the first day of treatment (day 7 after tumor inoculation). Each point represents the mean ± SD ($n = 5$). **$P < 0.01$ compared to the group treated with BL + US (Non-depletion). BL: Bubble liposomes, US: Ultrasound.

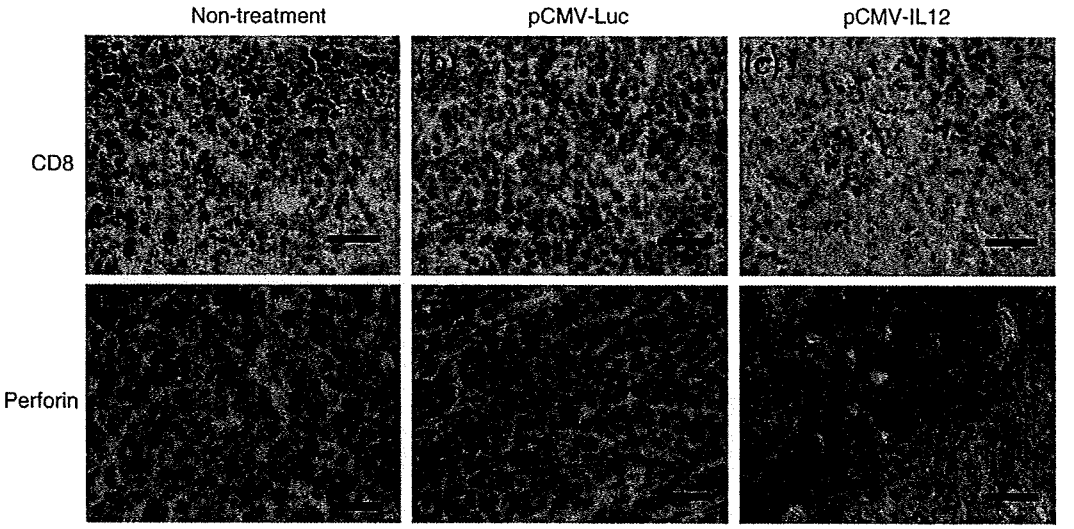

Fig. 5. Images of infiltrating T cells in OV-HM tumors following pCMV-IL12 delivery using Bubble liposomes and ultrasound. B6C3F1 mice were intradermally inoculated with 1×10^6 OV-HM cells into the flank. Seven, 9 or12 days after tumor inoculation, the tumors were injected with pCMV-Luc (b and e) or pCMV-IL12 (c and f) using Bubble liposomes and ultrasound. On day 13 after tumor inoculation, immunohistochemical staining against CD8 (a, b and c) and perforin (d, e and f) was performed using frozen tumor sections. Scale bar shows 10 μm.

an effective immunotherapeutic approach with reduced systemic adverse effects. Many anti-tumor effects depend on this method for IL-12 gene delivery. Viral vector systems have high potency and are effective for gene delivery, but gene therapy using viral vector systems may have associated safety issues [32]. Although transfection efficiency of most non-viral vector systems is lower, they are generally considered safer than viral vector systems [33]. Therefore, non-viral vector systems are preferred to cancer gene therapy using cytokines because it is not necessary to deliver the cytokine gene into all the cells. There have been many recent reports about gene delivery using the combination of nano/microbubbles and ultrasound [16–18], but most of them only confirmed the efficiency of gene expression using reporter genes. On the other hand, there have been few reports regarding therapeutic effects using sonoporation technology in cancer gene therapy. In this study, we assessed the effectiveness of the combination of Bubble liposomes and ultrasound as a non-viral vector system for effective cancer gene therapy, using plasmid DNA expressing IL-12, a potent primer of anti-tumor immunity.

IL-12 expression by IL-12 corded plasmid DNA delivery with the combination of Bubble liposomes and ultrasound was higher than that with a conventional lipofection method using Lipofectamine 2000 (Fig. 2). The therapeutic effect of IL-12 cancer gene therapy using each gene delivery method was compared (Fig. 3). IL-12 gene delivery with Lipofectamine 2000 did not suppress tumor growth, whereas gene delivery using a combination of Bubble liposomes and ultrasound effectively suppressed tumor growth. We originally thought that this was due to the level of IL-12 expression (Fig. 2), but complete tumor rejection was not observed in any mice treated with IL-12 gene delivery using Bubble liposomes and ultrasound (Fig. 3a), perhaps because the IL-12 gene is only transiently expressed in the tumor tissue. To address this problem, the IL-12 gene was repeatedly delivered using Bubble liposomes and ultrasound: as shown in Fig. 3b, the tumors were completely rejected. This complete rejection was attributed to the maintenance of therapeutic IL-12 levels in the tumor tissue. On the other hand, we could not observe anti-tumor effect in the luciferase corded plasmid DNA (pCMV-Luc) delivery with Bubble liposomes and ultrasound. This result not only suggests that IL-12 expression was important to suppress tumor growth but also suggests that there was no effect on tumor suppression by the combination of Bubble liposomes and ultrasound. In addition, we used Lipofectamine 2000 as control because gene transfection with intraperitoneal injection of Lipofectamine 2000 could effectively deliver into ascites tumor cells in our previous report [20]. Therefore, in this case of local tumoral injection, we thought that Lipofectamine 2000 could also be utilized as control vector system. Moreover, our collaborator reported about anti-tumor effects by single intratumoral injection of IL-12 expressing RGD fiber mutant adenovirus vector in OV-HM tumor bearing mice. In the report, tumor growth was suppressed and the tumor regression rate was about 40% [9]. In our study, although effective tumor growth suppression was observed in the therapeutic mice by single injection of IL-12 gene with Bubble liposomes and ultrasound, the tumor regressing mice were not observed. In this single therapy, our system was not equal to adenovirus vector in terms of tumor regression rate. On the other hand, the tumor regression rate in our repetitive therapy reached to 80%. And anti-tumor effect by repetitive therapy in our gene delivery system could go beyond that by single therapy with adenovirus vector. From these results, it was thought that the combination of Bubble liposomes and ultrasound might be a useful non-viral vector system for cancer gene therapy.

The anti-tumor effect by gene delivery with the combination of Bubble liposomes and ultrasound completely disappeared in mice lacking $CD8^+$ T lymphocytes (Fig. 4). Therefore, in this IL-12 gene therapy, $CD8^+$ T lymphocytes play a major role in suppressing tumor growth, suggesting that the combination of Bubble liposomes and ultrasound can effectively induce sufficient IL-12 expression to cause anti-tumor immune responses. In the Fig. 4, $CD8^+$ T lymphocytes depletion and $CD4^+$ and $CD8^+$ T lymphocytes depletion rather enhanced tumor growth. We thought that this reason was a same phenomenon as increasing the frequency of tumor generation according to decrease anti-tumor activity of immune competent cells by immunosuppressive agents. In brief, the balance of tumor growth and tumor rejection by immune system trend toward tumor growth by the depletion of $CD4^+$ and $CD8^+$ T lymphocytes. Therefore, it was thought that tumor growth was accelerated by the depletion. In other report, same phenomenon was observed [34]. The invasion of many $CD8^+$ T lymphocytes was observed in tumor tissue from mice treated with the IL-12 gene, Bubble liposomes and ultrasound (Fig. 5c), and perforin-positive cells were also observed in this tumor tissue (Fig. 5f). These results suggest that the expression of IL-12 genes, delivered using Bubble liposomes and ultrasound, primed the anti-tumor immunity, causing the tumor cells to be rejected. In this study, we did not measure the IL-12 concentration in the tumor tissue, but Colombo et al. reported that 30–80 pg/ml IL-12 at the tumor site can induce 40% regression of

C26 colon carcinoma [8]. Although the therapeutic effect depends on the type of cancer, we estimate that IL-12 concentrations of the order of tens of pg/ml are expressed at the tumor site using the present therapeutic system.

In conclusion, we demonstrated that the combination of Bubble liposomes and ultrasound effectively delivers the IL-12 gene into tumor tissue, and that local IL-12 production induces an immune response to the tumor cells. Therefore, the combination of Bubble liposomes and ultrasound could be a useful non-viral vector system in cancer gene therapy.

Acknowledgements

We thank Dr. Hiroshi Yamamoto (Department of Immunology, Graduate School of Pharmaceutical Sciences, Osaka University, Japan) for providing mIL-12 BIA/pBluescript II KS(−). We are grateful to Dr. Katsuro Tachibana (Department of Anatomy, School of Medicine, Fukuoka University, Japan) and Dr. Nobuki Kudo (Laboratory of Biomedical Instrumentation and Measurements, Graduate School of Information Science and Technology, Hokkaido University, Japan) for technical advice regarding the induction of cavitation with ultrasound exposure, to Dr. Yasuhiro Matsumura (Investigative Treatment Division, Research Center for Innovative Oncology, National Cancer Center Hospital East, Japan) for technical advice about cancer therapy, to Mr. Yasuyuki Shiono, Mr. Ryo Tanakadate, Mr. Kunihiko Matsuo, Mr. Ken Osawa and Ms. Motoka Kawamura (Department of Biopharmaceutics, School of Pharmaceutical Sciences, Teikyo University, Japan) for technical assistance, and to Mr. Yasuhiko Hayakawa, Mr. Takahiro Yamauchi and Mr. Kosho Suzuki (Nepa Gene Co., Ltd., Chiba, Japan) for technical advice about ultrasound exposure.

This study was supported by Grant-in-Aid for Young Scientists (B) from the Ministry of Education, Culture, Sports, Science and Technology of Japan, Grant-in-Aid for Scientific Research (A) and (B) from the Japan Society for the Promotion of Science, and Health and Labour Sciences Research Grants, Third Term Comprehensive Control Research for Cancer from the Ministry of Health, Labour and Welfare.

References

[1] U. Gubler, A.O. Chua, D.S. Schoenhaut, C.M. Dwyer, W. McComas, R. Motyka, N. Nabavi, A.G. Wolitzky, P.M. Quinn, P.C. Familletti, Coexpression of two distinct genes is required to generate secreted bioactive cytotoxic lymphocyte maturation factor, Proc Natl Acad Sci U S A 88 (1991) 4143–4147.
[2] S.F. Wolf, P.A. Temple, M. Kobayashi, D. Young, M. Dicig, L. Lowe, R. Dzialo, L. Fitz, C. Ferenz, R.M. Hewick, Cloning of cDNA for natural killer cell stimulatory factor, a heterodimeric cytokine with multiple biologic effects on T and natural killer cells, J Immunol 146 (1991) 3074–3081.
[3] M.J. Brunda, Interleukin-12, J Leukoc Biol 55 (1994) 280–288.
[4] C.L. Nastala, H.D. Edington, T.G. McKinney, H. Tahara, M.A. Nalesnik, M.J. Brunda, M.K. Gately, S.F. Wolf, R.D. Schreiber, W.J. Storkus, Recombinant IL-12 administration induces tumor regression in association with IFN-gamma production, J Immunol 153 (1994) 1697–1706.
[5] W.G. Yu, M. Ogawa, J. Mu, K. Umehara, T. Tsujimura, H. Fujiwara, T. Hamaoka, IL-12-induced tumor regression correlates with in situ activity of IFN-gamma produced by tumor-infiltrating cells and its secondary induction of anti-tumor pathways, J Leukoc Biol 62 (1997) 450–457.
[6] M.B. Atkins, M.J. Robertson, M. Gordon, M.T. Lotze, M. DeCoste, J.S. DuBois, J. Ritz, A.B. Sandler, H.D. Edington, P.D. Garzone, J.W. Mier, C.M. Canning, L. Battiato, H. Tahara, M.L. Sherman, Phase I evaluation of intravenous recombinant human interleukin 12 in patients with advanced malignancies, Clin Cancer Res 3 (1997) 409–417.
[7] J.P. Leonard, M.L. Sherman, G.L. Fisher, L.J. Buchanan, G. Larsen, M.B. Atkins, J.A. Sosman, J.P. Dutcher, N.J. Vogelzang, J.L. Ryan, Effects of single-dose interleukin-12 exposure on interleukin-12-associated toxicity and interferon-gamma production, Blood 90 (1997) 2541–2548.
[8] M.P. Colombo, M. Vagliani, F. Spreafico, M. Parenza, C. Chiodoni, C. Melani, A. Stoppacciaro, Amount of interleukin 12 available at the tumor site is critical for tumor regression, Cancer Res 56 (1996) 2531–2534.
[9] J.Q. Gao, T. Sugita, N. Kanagawa, K. Iida, Y. Eto, Y. Motomura, H. Mizuguchi, Y. Tsutsumi, T. Hayakawa, T. Mayumi, S. Nakagawa, A single intratumoral injection of a fiber-mutant adenoviral vector encoding interleukin 12 induces remarkable anti-tumor and anti-metastatic activity in mice with Meth-A fibrosarcoma, Biochem Biophys Res Commun 328 (2005) 1043–1050.
[10] Y. Gao, Z. Xu, S. Chen, W. Gu, L. Chen, Y. Li, Arginine-chitosan/DNA self-assemble nanoparticles for gene delivery: in vitro characteristics and transfection efficiency, Int J Pharm 359 (2008) 241–246.
[11] H. Hatakeyama, H. Akita, K. Kogure, M. Oishi, Y. Nagasaki, Y. Kihira, M. Ueno, H. Kobayashi, H. Kikuchi, H. Harashima, Development of a novel systemic gene delivery system for cancer therapy with a tumor-specific cleavable PEG-lipid, Gene Ther 14 (2007) 68–77.
[12] T. Montier, T. Benvegnu, P.A. Jaffres, J.J. Yaouanc, P. Lehn, Progress in cationic lipid-mediated gene transfection: a series of bio-inspired lipids as an example, Curr Gene Ther 8 (2008) 296–312.
[13] M. Morille, C. Passirani, A. Vonarbourg, A. Clavreul, J.P. Benoit, Progress in developing cationic vectors for non-viral systemic gene therapy against cancer, Biomaterials 29 (2008) 3477–3496.
[14] M. Fechheimer, J.F. Boylan, S. Parker, J.E. Sisken, G.L. Patel, S.G. Zimmer, Transfection of mammalian cells with plasmid DNA by scrape loading and sonication loading, Proc Natl Acad Sci U S A 84 (1987) 8463–8467.
[15] M.W. Miller, D.L. Miller, A.A. Brayman, A review of in vitro bioeffects of inertial ultrasonic cavitation from a mechanistic perspective, Ultrasound Med Biol 22 (1996) 1131–1154.
[16] C.M. Newman, T. Bettinger, Gene therapy progress and prospects: ultrasound for gene transfer, Gene Ther 14 (2007) 465–475.
[17] Z.P. Shen, A.A. Brayman, L. Chen, C.H. Miao, Ultrasound with microbubbles enhances gene expression of plasmid DNA in the liver via intraportal delivery, Gene Ther 15 (2008) 1147–1155.
[18] Y. Taniyama, K. Tachibana, K. Hiraoka, T. Namba, K. Yamasaki, N. Hashiya, M. Aoki, T. Ogihara, K. Yasufumi, R. Morishita, Local delivery of plasmid DNA into rat carotid artery using ultrasound, Circulation 105 (2002) 1233–1239.
[19] R. Suzuki, T. Takizawa, Y. Negishi, K. Hagisawa, K. Tanaka, K. Sawamura, N. Utoguchi, T. Nishioka, K. Maruyama, Gene delivery by combination of novel liposomal bubbles with perfluoropropane and ultrasound, J Control Release 117 (2007) 130–136.
[20] R. Suzuki, T. Takizawa, Y. Negishi, N. Utoguchi, K. Sawamura, K. Tanaka, E. Namai, Y. Oda, Y. Matsumura, K. Maruyama, Tumor specific ultrasound enhanced gene transfer in vivo with novel liposomal bubbles, J Control Release 125 (2008) 137–144.
[21] R. Suzuki, Y. Oda, N. Utoguchi, E. Namai, Y. Taira, N. Okada, N. Kadowaki, T. Kodama, K. Tachibana, K. Maruyama, A novel strategy utilizing ultrasound for antigen delivery in dendritic cell-based cancer immunotherapy, J Control Release 133 (2009) 198–205.
[22] T. Yamashita, S. Sonoda, R. Suzuki, N. Arimura, K. Tachibana, K. Maruyama, T. Sakamoto, A novel bubble liposome and ultrasound-mediated gene transfer to ocular surface: RC-1 cells in vitro and conjunctiva in vivo, Exp Eye Res 85 (2007) 741–748.
[23] Y. Negishi, Y. Endo, T. Fukuyama, R. Suzuki, T. Takizawa, D. Omata, K. Maruyama, Y. Aramaki, Delivery of siRNA into the cytoplasm by liposomal bubbles and ultrasound, J Control Release 132 (2008) 124–130.
[24] K. Un, S. Kawakami, R. Suzuki, K. Maruyama, F. Yamashita, M. Hashida, Enhanced transfection efficiency into macrophages and dendritic cells by the combination method using mannosylated lipoplexes and Bubble liposomes with ultrasound exposure Hum Gene Ther. (2009) In press.
[25] M. Hashimoto, O. Niwa, Y. Nitta, M. Takeichi, K. Yokoro, Unstable expression of E-cadherin adhesion molecules in metastatic ovarian tumor cells, Jpn J Cancer Res 80 (1989) 459–463.
[26] Y. Okada, N. Okada, S. Nakagawa, H. Mizuguchi, M. Kanehira, N. Nishino, K. Takahashi, N. Mizuno, T. Hayakawa, T. Mayumi, Fiber-mutant technique can augment gene transduction efficacy and anti-tumor effects against established murine melanoma by cytokine-gene therapy using adenovirus vectors, Cancer Lett 177 (2002) 57–63.
[27] C. Fillat, M. Carrio, A. Cascante, B. Sangro, Suicide gene therapy mediated by the Herpes Simplex virus thymidine kinase gene/Ganciclovir system: fifteen years of application, Curr Gene Ther 3 (2003) 13–26.
[28] X.H. Shi, Z.Y. Liang, X.Y. Ren, T.H. Liu, Combined silencing of K-ras and Akt2 oncogenes achieves synergistic effects in inhibiting pancreatic cancer cell growth in vitro and in vivo, Cancer Gene Ther 16 (2009) 227–236.
[29] M. Nogawa, T. Yuasa, S. Kimura, M. Tanaka, J. Kuroda, K. Sato, A. Yokota, H. Segawa, Y. Toda, S. Kageyama, T. Yoshiki, Y. Okada, T. Maekawa, Intravesical administration of small interfering RNA targeting PLK-1 successfully prevents the growth of bladder cancer, J Clin Invest 115 (2005) 978–985.
[30] C.W. Beh, W.Y. Seow, Y. Wang, Y. Zhang, Z.Y. Ong, P.L. Ee, Y.Y. Yang, Efficient delivery of Bcl-2-targeted siRNA using cationic polymer nanoparticles: down-regulating mRNA expression level and sensitizing cancer cells to anticancer drug, Biomacromolecules 10 (2009) 41–48.
[31] M. Folini, M. Pennati, N. Zaffaroni, RNA interference-mediated validation of genes involved in telomere maintenance and evasion of apoptosis as cancer therapeutic targets, Methods Mol Biol 487 (2009) 303–330.
[32] S. Lehrman, Virus treatment questioned after gene therapy death, Nature 401 (1999) 517–518.
[33] C.C. Conwell, L. Huang, Recent advances in non-viral gene delivery, Adv Genet 53PA (2005) 1–18.
[34] N. Kanagawa, J.Q. Gao, Y. Motomura, T. Yanagawa, Y. Mukai, Y. Yoshioka, N. Okada, S. Nakagawa, Antitumor mechanism of intratumoral injection with IL-12-expressing adenoviral vector against IL-12-unresponsive tumor, Biochem Biophys Res Commun 372 (2008) 821–825.

Journal of Electron Microscopy Advance Access published November 11, 2009

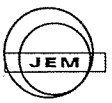

Journal of Electron Microscopy: 1–10 (2009)
doi: 10.1093/jmicro/dfp056

Physical: Full-length—Experimental

Morphological study of acoustic liposomes using transmission electron microscopy

Tetsuya Kodama[1,*], Noriko Tomita[1,5], Sachiko Horie[1], Nicolas Sax[1], Hiroko Iwasaki[1], Ryo Suzuki[2], Kazuo Maruyama[2], Shiro Mori[3] and Fukumoto Manabu[4]

[1]Graduate School of Biomedical Engineering, Tohoku University, 2-1 Seiryo, Aoba, Sendai, 980-8575, Japan, [2]Department of Biopharmaceutics, School of Pharmaceutical Sciences, Teikyo University, 1091-1 Suwarashi, Sagamiko, Sagamihra, Kanagawa, 229-0195, Japan, [3]Department of Oral Health Science, Tohoku University Hospital, 1-1 Seiryo, Aoba, Sendai, 980-8574, Japan and [4]Institute of Development, Aging and Cancer, Tohoku University, 4-1 Seiryo, Aoba, Sendai, 980-8575, Japan
[5]Present address: Institute of Fluid Science, Tohoku University, 2-1-1 Katahira, Aoba, Sendai, 980-8577, Japan
*To whom correspondence should be addressed. E-mail: kodama@bme.tohoku.ac.jp

Abstract Sonoporation is achieved by ultrasound-mediated destruction of ultrasound contrast agents (UCA) microbubbles. For this, UCAs must be tissue specific and have good echogenicity and also function as drug carriers. Previous studies have developed acoustic liposomes (ALs), liposomes that encapsulate phosphate buffer solution and perfluoropropane (C_3F_8) gas and function as both UCAs and drug carriers. Few studies have examined the co-existence of gas and liquid in ALs. This study aims to elucidate AL structure using TEM. The size, zeta potential and structure of ALs were compared with those of two other UCAs, human albumin shell bubbles (ABs; Optison) and lipid bubbles (LBs). ABs and LBs encapsulate the C_3F_8 gas. Particle size was measured by dynamic light scattering. The zeta potential was determined by the Smoluchowski equation. UCA structure was investigated by TEM. ALs were ~200 nm in size, smaller than LBs and ABs. ALs and LBs had almost neutral zeta potentials whereas AB values were strongly negative. The negative or double staining TEM images revealed that ~20% of ALs contained both liquid and gas, while ~80% contained liquid alone (i.e. nonacoustic). Negative staining AB images indicated electron beam scattering near the shell surface, and albumin was detected in filament form. These findings suggest that AL is capable of carrying drugs and high-molecular-weight, low-solubility gases.

Keywords nanobubbles, drug delivery system, sonoporation, ultrasound contrast agent, cavitation

Received 25 June 2009, accepted 5 October 2009

Introduction

Ultrasound contrast agents (UCAs) are nano/microbubbles that contain air or a high-molecular-weight, low water-solubility gas (e.g. C_3F_8, C_4F_{10} and SF_6) encapsulated in a lipid or albumin shell [1–6]. The diameters of UCAs vary from 100 nm to 10 μm and their behavior primarily depends on the ultrasound characteristics. The behavior of UCAs is described by an equation of motion that consists of external force, viscosity and stiffness terms [7]. When the external force is small, i.e. ultrasound pressure is small, UCAs undergo small volumetric oscillation (linear). With increasing ultrasound pressures, the amplitude of volumetric oscillation increases and

oscillation becomes aperiodic (nonlinear), resulting in destruction of UCAs [1,8].

Drug delivery via sonoporation using ultrasound and UCAs is a technique used for diagnosis and treatment [1,8] and is based on bubble destruction modes. During sonoporation, primary UCAs and subsequent bubble cavitation generated by the collapse of the UCAs induce mechanical forces such as liquid jets and shock waves [8]. These forces interact with the surrounding cells, resulting in the permeation of exogenous molecules into cells [1,8]. Sonoporation is a noninvasive, nonimmunogenic and tissue-specific procedure that has been used to treat cancer and many other diseases [1,3,9]. However, the efficiency of molecular delivery is relatively low; therefore, it has not been recognized as a clinically valuable approach. One strategy towards improving the efficiency of molecular delivery is to develop UCAs that are tissue-specific and that can function as drug carriers. Suzuki *et al.* [9] developed a novel form of liposome containing the C_3F_8 gas and phosphate buffer solution and demonstrated that it functions as an acoustic liposome (AL) applicable to a nonvirus molecular delivery system [5,6]. The liposome surface was covered with polyethyleneglycol (PEG); therefore, it was assumed that this molecule would not be incorporated by the reticuloendothelial system, thereby allowing a longer retention in the blood [10]. In addition, the tumor-targeting potential and drug-carrying capability are significantly improved by conjugating PEG with ligands specific for the target tissue and by producing bubbles with diameters of <100 nm, which allows for enhanced permeability and retention (EPR) effects [11,12]. These studies concluded that the liposome would be acoustic due to the differences between ultrasound backscatter intensities in the presence/absence of ultrasound. However, the coexistence of gas and liquid in the liposome has not been examined, neither have its size and structure been discussed.

The present study investigated the size, zeta potential and structure of ALs and compared these values with those of two other types of UCAs: a single human albumin shell (ABs; Optison) and lipid bubbles (LBs). Both UCAs encapsulated the C_3F_8 gas, which was identical to the liposome gas. Transmission electron microscopy (TEM) was used to assess the structure of UCAs, and the TEM images were obtained using either negative or double staining. The TEM findings will be used as parameters to evaluate biodistribution, safety and efficacy of micro/nanoparticulate systems.

Methods

Nano/microbubble preparation

Three types of UCA—ABs ($5.0–8.0 \times 10^8$ bubbles mL^{-1}; Optison™, Amersham Health Plc, Oslo, Norway), LBs and ALs—were used. LBs were created in an aqueous dispersion of 2 mg mL^{-1} 1,2-distearoyl-sn-glycero-phosphatidylcholine (DSPC) (Avanti Polar Lipids, Alabaster, AL, USA) and 1 mg mL^{-1} polyethylene glycol (PEG) distearate (Sigma-Aldrich) using a 20 kHz stick sonicator (130 W, Vibra Cell, Sonics & Materials Inc., Danbury, CT, USA) at 50% amplifying strength for 1 min, in the presence of C_3F_8 gas in a sterilized 7 mL Bijou vial [8,13,14]. The vial cap has two openings that serve as a gas inlet and outlet. During sonication, the C_3F_8 gas was kept under the condition of inflow and outflow through the openings. The LB concentration was 3.4×10^8 bubbles mL^{-1} [13]. ALs were prepared by modifying the protocol of Suzuki *et al.* [9]. First, DSPC (NOF Co., Tokyo, Japan) and 1,2-distearoyl-sn-glycero-3-phosphatidyl-ethanolamine-methoxy-polyethyleneglycol (DSPE-PEG2000-OMe) (NOF Co.) (94:6 [mol/mol]) were dissolved in 10 mL of 9:1 (v/v) chloroform/methanol. Next, 5 mL of phosphate-buffered saline (PBS) without Mg^{2+} and Ca^{2+} (pH 7.2 at room temperature, Sigma) was added to the solution. The solution was then sonicated using a 20 kHz stick sonicator (Sonics & Materials). Liposomes were obtained by reverse phase evaporation at 65°C. The organic solvent was completely removed, and the size of the liposomes was adjusted to <100 nm using extruding equipment (Northern Lipids Inc., Vancouver, BC, Canada) with three sizing filters (pore sizes: 100, 200 and 600 nm) (Nuclepore Track-Etch Membrane, Whatman plc, UK). The resulting liposomes were passed through a 0.45 μm pore size filter (MILLEX HV filter unit, Durapore polyvinylidine-difluoride (PVDF) membrane, Millipore Corporation, MA, USA) for sterilization. Lipid concentration was measured using the Phospholipid *C*-test Wako (Wako Pure Chemical Industries, Ltd, Osaka, Japan). To produce AL, a

liposome suspension of 1 mL (lipid concentration: 1 mg mL^{-1}) was sonicated using a bath sonicator (42 kHz, 100 W; Bransonic 2510J-DTH, Branson Ultrasounics Co., Danbury, CT, USA) and a 20 kHz stick sonicator (130 W, Sonics & Materials, Inc.) at 50% amplifying strength for 1 min, in the presence of C_3F_8 in a sterilized 7 mL Bijou vial, as described above.

Dark field microscopy

Immediately after sonication, 20 μL drops of either AL or LB were put on a glass cover and were observed under an inverted microscope (IX81, Olympus, Tokyo, Japan) equipped with an illuminator (Darlkite Illuminator, Micro Video Instruments, Avon, MA , USA).

Echogenicity measurement

The air inside the 5 mL vials containing 1 mL of liposome suspension (lipid concentration: 1 mg mL^{-1}) sealed with a rubber cap together with an aluminium jacket was replaced with 12 mL of air or C_3F_8 gas and supercharged with another 12 mL of each gas. The suspension in the vial was sonicated in a bath sonicator (Branson Ultrasounics) for 2 min. The suspension was transferred to a 7 mL Bijou vial and further sonicated by a 20 kHz sonicator (Sonics & Materials) at 50% amplifying strength for 1 min while 5 mL of each gas was injected at a rate of 300 mL h^{-1} using a syringe pump (model KDS 100, KD Scientific, Holliston, MA, USA). Four milliliters of a 40-fold dilution with PBS were added to a well of a 6-well plate and the B-mode image was acquired with a high-frequency ultrasound imaging system with a center frequency of 55 MHz (VEVO 770, Visualsonics Inc., Toronto, Canada). The grayscale histogram of a selected ROI was measured using the implemented software of the US imaging system. The ROI circle was set to 1.00 mm^2, 1 mm above the bottom of the well.

Size and zeta potential

The size and zeta potentials of the bubbles were measured using a zeta potential & particle size analyzer (zeta potential range: −200 to +200 mV, particle size/distribution range: 0.6 nm to 7 μm, laser source: laser diode (660 nm), ELSZ-2, Otsuka Electronics, Osaka, Japan). The size was measured using the dynamic light scattering. The zeta potential was automatically calculated on the basis of the electrophoretic mobility using the Smoluchowski equation: $\zeta = 4\pi\eta u/\varepsilon$, where ζ is the zeta potential, u is the electrophoretic mobility and η and ε are the viscosity and dielectric constant of the solvent, respectively. The Smoluchowski equation is applicable to a solid surface on which a surface-charge layer exits and electrolyte ions do not penetrate through the surface, i.e. hard particles [15]. In the present study, the three types of bubbles were assumed to be hard particles. The bubble solutions were diluted in PBS to $\sim 10^7$ bubbles mL^{-1} at room temperature (21–23°C). The average values of the sizes and zeta potentials were calculated using four to nine independent measurements on each sample.

TEM

Either negative or double staining was used for AL. Negative staining was used for LB and AB. The stained samples were examined with a JEM-2000EX operated at 100 kV (JEOL Datum, Tokyo, Japan) at the Hanaichi UltraStructure Research Institute, Aichi, Japan; or with a H-7600 operated at 80 kV (Hitachi Tokyo, Japan) at Tohoku University, Sendai, Japan. For the negative staining, a 400-mesh grid (EM fine-grid F-400, Nisshin EM Co., Tokyo, Japan) with a carbon support film (10–20 nm in thickness) was used, and was given a hydrophilic treatment. Samples were stained at either room temperature or at 80°C. For the former case, a drop of sample solution, distilled water and phosphotungstic acid (Merck, Tokyo, Japan) were put on a parafilm (Pechiney Plastic Packaging Co., Menasha, WI, USA). The grid was put into the sample drop (30 s), then in a distilled water drop for washing (10 s) and finally in a phosphotungstic acid drop for staining (10 s). Any excess solution was removed with filter paper. For the latter case, a parafilm was floated on water heated at 80 °C, and the procedure outlined above was then followed. For the double staining, an AL solution generated in the presence of C_3F_8 in a sterilized 7 mL vial was immediately added to 1 mL of 2% agarose (Cambrex Bio Science Rockland, Inc., Rockland, USA) to obtain a stable solution that did not release gas. Then, the AL solution was mixed with the same amount of

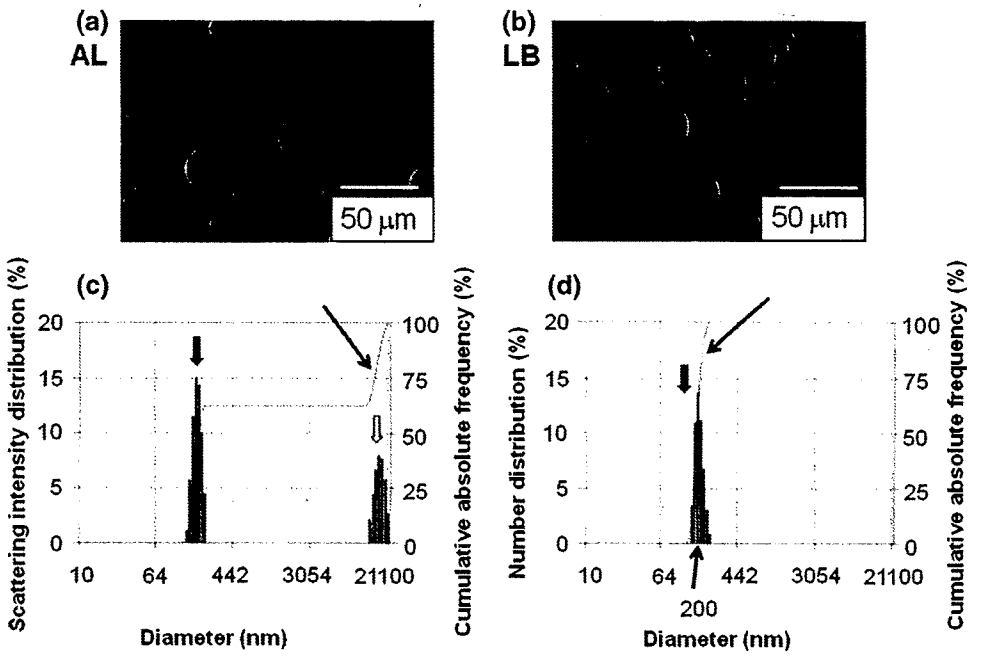

Fig. 1. Dark field images of ALs and LBs and size distribution of ALs. (a) AL dark field image. (b) LB dark field image. (c) Scattering intensity distribution (%) and cumulative absolute frequency (%) of ALs, measured using dynamic light scattering. There are two peaks indicating diameters of ~200 nm (⇓) and 15 700 nm (⇩). (d) Number distribution (%) and cumulative absolute frequency (%) of AL, measured by dynamic light scattering. Approximately 100% of ALs were ~200 nm in diameter (⇓). ALs with diameters exceeding a few micrometers accounted for <0.01%. The arrows (↓) in (c) and (d) indicate the line of the cumulative absolute frequency (%).

2% osmium tetroxide solution, and was fixed at 4°C for 6 h. Dehydration in an ethanol series (50–100%) at room temperature followed, and the solution was embedded in an EPON812 resin mixture at 60°C for 48 h. Thin sections were obtained using an ultramicrotome (Power Tome XL, RMC, Boekeler Instruments, Tucson, AZ, USA). They were stained with 2% uranyl acetate (Merck) for 15 min, washed with rinse solution and were finally stained with a lead stain solution (Sigma, Tokyo, Japan) for 5 min. Histogram of the absolute frequency distribution was obtained from 10 TEM images. The diameter of each AL was measured with rulers.

Brightness analysis

Two sets of TEM images (ALs, and non-gas-containing liposomes [LSs]) were analyzed to assess the average brightness value of the inside of each kind of liposome. The inner area of each liposome on the images was individually selected and its mean brightness value obtained by the ImageJ software (Rasband, W. S., Image J, U. S. NIH, Bethesda, MD, USA, http://rsb.info.nih.gov/ij/, 1997–2009.). For each image, a brightness value of the background was measured and used for normalization. Overstained areas were left out for both types of measurements. Relative brightness values (measured mean brightness/background brightness) were obtained for 106 LSs and 83 ALs.

Statistical analysis

All measurements were represented as either mean ± SD (standard deviation) or SEM (standard error of the mean). Statistical analysis was performed by using Student's *t*-test. Difference with $P < 0.05$ was considered significant. The statistical analysis was performed using Excel 2000 (Microsoft, USA) with the add-in software Statcel 2 [16].

Results

First, the data obtained for ALs and LBs using dark light microscopy were examined, given that both have similar membrane components (Fig. 1a and b). Figure 1a shows that each AL was captured clearly. ALs with a diameter of up to 30 μm existed. Figure 1c shows the percentage of scattering intensity distribution and cumulative absolute frequency of ALs. Two peaks were observed indicating diameters of ~200 nm and 15 700 nm. Figure 1d shows the

Table 1. Bubble characteristics

Nano/microbubble	Shell	Gas	[a]Size (nm)	[b]Zeta potential (mV)
AL	DSPC/DSPE-PEG2000	Perfluoropropane	199 ± 84.4 ($n = 8$)	-2.1 ± 0.9 ($n = 4$)
LB	DSPC/PEG	Perfluoropropane	1222 ± 442.7 ($n = 9$)	-4.2 ± 1.3 ($n = 5$)
AB (Optison)	Albumin	Perfluoropropane	1689 ± 299.8 ($n = 4$)	-40 ± 6.9 ($n = 4$)

[a]Size was measured using dynamic light scattering. Approximately 100% of ALs were ~200 nm in diameter. ALs with diameters larger than a few micrometers accounted for <0.01% (see Fig. 1). Further, 90% of the LBs were ~1200 nm in diameter (data not shown).
[b]The zeta potential was calculated using the Smoluchowski equation.
Values are represented as mean ± SD.

number distribution (%) and cumulative absolute frequency (%), which have been converted from Fig. 1c. Results show that most ALs have diameters of ~200 nm, while ALs with diameters exceeding a few micrometers accounted for <0.01% (Fig. 1c and d). Figure 1b shows the overall LB view. Although large bubbles were visible, the tiny bubbles that were observed in Fig. 1a were not detected in Fig. 1b. The mean diameters for the ALs, LBs and ABs are summarized in Table 1, with AL diameter being one digit smaller than that of the LBs and ABs.

To confirm that the C_3F_8 gas was actually encapsulated by the AL shell, we measured the echogenicity of liposomes sonicated in the presence of either atmospheric air or C_3F_8 gas. Figure 2a shows characteristics of liposomes under either atmospheric air or C_3F_8 gas. Photos show that liposome suspension sonicated in the presence of C_3F_8 is cloudier than that of air and original liposome suspension (NONE). Next we measured echogenicity of each bubble by the method indicated in Fig. 2c. The US B-mode images show that liposome sonicated in the presence of the C_3F_8 gas have a high echogenicity. This tendency is confirmed by the brightness histogram of the liposome sonicated in the presence of the C_3F_8 gas that displays a shift to the right of the brightness levels compared to that with air. Figure 2b indicates the difference of brightness value between liposome sonicated in the presence of either atmospheric air or C_3F_8 gas. The values were normalized by that of NONE. There is a highly significant difference between them ($P < 0.01$).

The zeta potential is one of the primary parameters indicative of drug delivery efficiency, since it informs about dispersivity, aggregability and mutual interaction inside the colloidal suspension. Zeta potential values are summarized in Table 1. ALs and LBs possessed neutral values since neutral lipid phosphatidylcholine was the primary component of their shells and the PEG distributed on their shell surfaces is a nonelectrolyte, water-soluble polymer. ABs had a strong negative charge, indicating that the AB colloid is the most stable of the three bubble types.

Next, ALs were stained using negative staining, and their structures were examined by TEM (Fig. 3). In general, when a lipid bilayer is negatively stained, the stain solution penetrates the lipid bilayer. Existence of gas within certain areas of ALs will prevent that area from being stained effectively, resulting in a reduction in net electron density in that area. The black arrows in Fig. 3a and b indicate the presence of gas within the ALs. Decreased electron density in the central area was apparent in 69 out of 345 ALs, i.e. 20%. The shape of LBs (Fig. 3c and d) was not always spherical as compared to the shapes of ALs. A significant decrease in electron density was not observed in the interior making it difficult to determine whether gas existed in the LB. Figure 3d shows that some LBs had a bag configuration suggesting that an LB may potentially contain both gas and liquid. The AB shell structure caused strong electron beam scattering around the shell (Fig. 3e). As shown in the magnified figure (Fig. 3f), albumin was observed in filament form (indicated by the black arrow), with the layer being several hundred nanometers thick. The interior gas was assumed to be packed in a stable manner and covered with the thick albumin shell. The internal electron density was relatively low, indicating the existence of gas. Figure 4 shows the histogram of the absolute frequency distribution obtained from 10 TEM micrographs. The maximum value was obtained within the class interval of 91–120 nm. This value was about half that measured with dynamic light scattering (see Table 1). Figure 5 shows the distribution of relative brightness values in original liposomes (LSs) and ALs. The statistical distribution of ALs is slightly shifted to relative brightness values closer to 1 compared to the

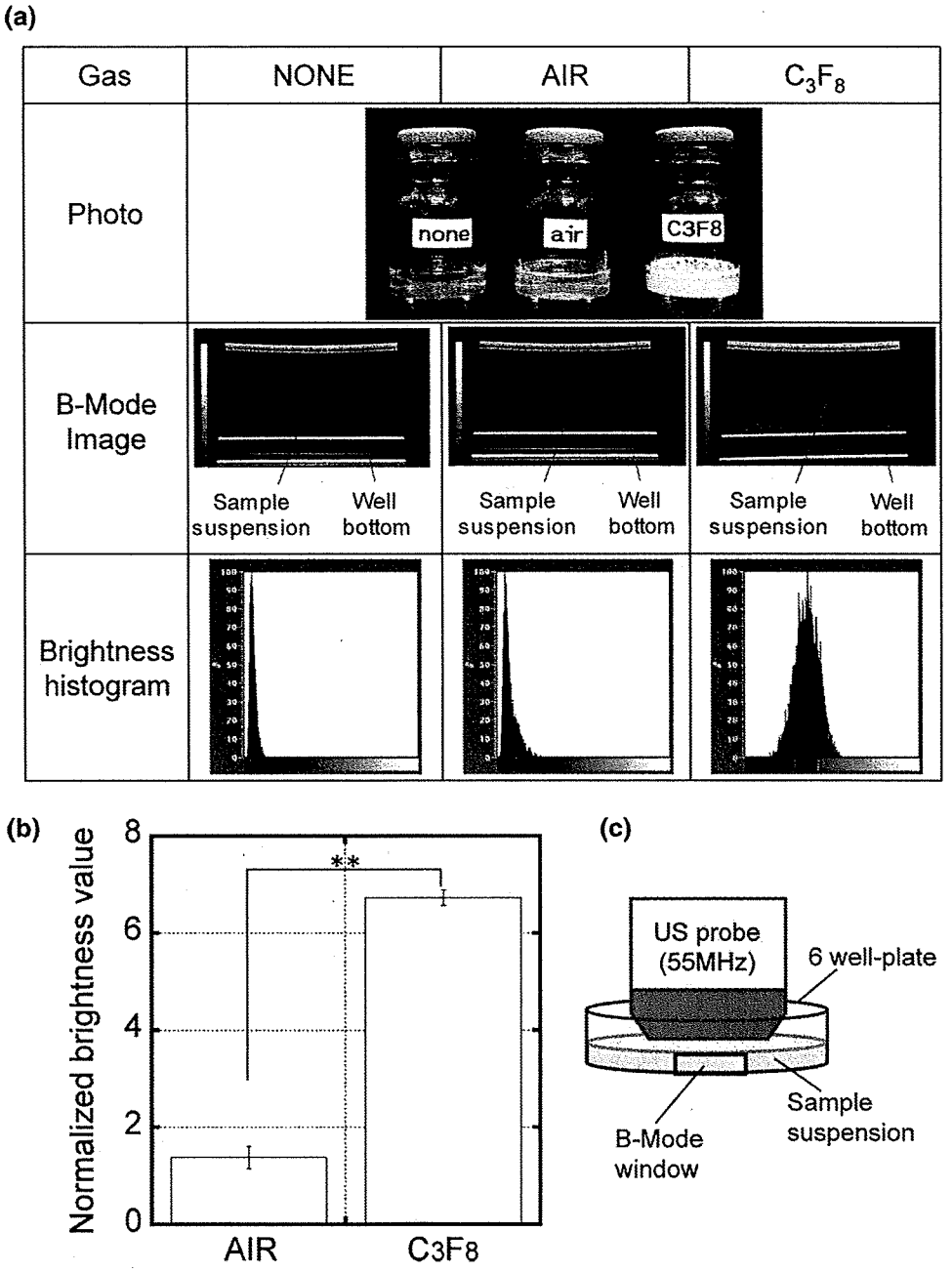

Fig. 2. Confirmation of gas entrapment into liposome. Photos, US B-mode images and brightness histograms of original liposome suspension (none), liposome sonicated under either atmospheric air (air) or C_3F_8 gas (C_3F_8) indicate encapsulation of gas under the presence of the C_3F_8 gas but not in the presence of air (a). The US B-mode images were captured as shown in the scheme for ultrasound imaging (c). There was a highly significant difference in brightness value between liposome sonicated under atmospheric air and C_3F_8 gas. The values were normalized with that of liposome without gas. $n = 4$, mean ± S.E. $^{**}P < 0.01$.

distribution of LSs, indicating that C_3F_8 gas bubbles are actually present inside some of the ALs.

Figure 6 shows a magnified image of the AL, stained at 80°C with the negative staining. The fluidity of lipid layers increases due to heat, and results in the enhanced penetration of the staining solution. The shell thickness was 5.6 nm, which accords with a biomembrane with a thickness of 7–10 nm. Thus, the AL shell is assumed to be a single lipid bilayer.

In order to investigate the AL structure in detail, we observed its cross-section, obtained from the double staining (Fig. 7). The black arrows in Fig. 7a indicate the presence of gas, while the white arrow indicates the presence of liquid. The percentage of